A FEEDBACK LINEARIZATION APPROACH FOR PANEL FLUTTER

SUPPRESSION WITH PIEZOELECTRIC ACTUATION

Except where reference is made to the work of others, the work described in this dissertation is my own or was done in collaboration with my advisory committee. This dissertation does not include proprietary or classified information.

_____

Oluseyi Olasupo Onawola

Certificate of Approval:

_____	_____
Subhash C. Sinha, Co-Chair Professor Mechanical Engineering	Winfred A. Foster, Jr., Co-Chair Professor Aerospace Engineering
_____	_____
Robert S. Gross Associate Professor Aerospace Engineering	John Y. Hung Professor Electrical and Computer Engineering
_____	_____
Gilbert L. Crouse, Jr. Associate Professor Aerospace Engineering	George T. Flowers Dean Graduate School

A FEEDBACK LINEARIZATION APPROACH FOR PANEL FLUTTER SUPPRESSION WITH PIEZOELECTRIC ACTUATION

Oluseyi Olasupo Onawola

A Dissertation

Submitted to

the Graduate Faculty of

Auburn University

in Partial Fulfillment of the

Requirements for the

Degree of

Doctor of Philosophy

Auburn, Alabama
December 19, 2008

A FEEDBACK LINEARIZATION APPROACH FOR PANEL FLUTTER

SUPPRESSION WITH PIEZOELECTRIC ACTUATION

Oluseyi Olasupo Onawola

_____

Signature of Author

_____

Date of Graduation

DISSERTATION ABSTRACT

A FEEDBACK LINEARIZATION APPROACH FOR PANEL FLUTTER SUPPRESSION WITH PIEZOELECTRIC ACTUATION

Oluseyi Olasupo Onawola

Doctor of Philosophy, December 19, 2008
(M.S., University of Delaware, 2004)
(M.Eng., University of Ilorin, 1998)
(B.Sc., Obafemi Awolowo, 1990)

122 Typed Pages

Directed by Winfred A. Foster and Subhash C. Sinha

A panel is subject to dynamic instability when induced aerodynamic loads under the supersonic/hypersonic environment result in a self-excited oscillation called panel flutter. The panel of an aircraft that flies at supersonic speed or a structural panel that is in fluid flow at such regime may experience panel flutter. A plate with highly distributed piezoelectric actuators and sensors connected to processing networks, referred to as intelligent plate can actively control its vibrations. The objective of this research is to analytically demonstrate panel flutter suppression using piezoelectric actuation based on feedback linearization controllers.

A nonlinear control system is formulated using the nonlinear dynamic equations for a simply supported rectangular panel with piezoelectric layers based on Galerkin's method with modal expansions of nonlinear partial differential equation obtained from

von Kárman large-deflection plate theory, which accounts for the structure nonlinearity. The nonlinear equations also account for loads such as externally applied in-plane loads, aerodynamic loads, and electrical displacements. The aerodynamic loads are given by the first-order piston theory or the quasi-steady supersonic theory. The control inputs are given by the electric fields required to drive the actuators based on piezoelectric actuation, which is modeled by linear piezoelectric constitutive relations. Outputs of the nonlinear system are feedback and used to transform it into an equivalent controllable linear system in new coordinates by formulating nonlinear feedback control laws, which cancel the nonlinear dynamics resulting in a linear system. The pole placement technique is then employed to make the states of the feedback linearized models locally asymptotically stable at a given equilibrium.

Numerical simulations are carried out for the closed-loop systems at dynamic pressures higher than the critical dynamic pressures for the onset of panel flutter, where limit-cycle motions are generated. The simulated systems show that the closed-loop systems based on the controllers effectively suppress panel flutter limit-cycle motions with the generated piezoelectric bending actuations as control inputs. Therefore, with the feedback linearization controllers developed, the limit-cycle motion of panel flutter can be completely suppressed or the panel can be made flutter free if the controller gains are carefully selected.

ACKNOWLEDGMENTS

The author gives thanks to God in whom resides all knowledge, all wisdom, and all power; for it is He, who has made it so that order masquerades as randomness.

The author expresses his thanks to Dr. W. A. Foster and Dr. S. C. Sinha, my co-advisors, for creating the opportunity for me to work on this research. He is also gratefully indebted to them for their support, advice, and guidance. He would also like to thank Dr. J. Y. Hung, Dr. R. S. Gross, and Dr. G. L. Crouse for serving as members of his committee. He has found their advice, assistance, and contributions highly invaluable.

He acknowledges the roles played by the chair of the department, Dr. J. E. Cochran, and the office staff, Ms. Ginger Ware and Ms. Evia Vickerstaff, for creating conducive environment for this study. He also would like to thank Bob and Frances Stevenson, James and Cathey Donald, Dr. Henry Y. Fadamiro, Dr. Charlotte Ward, Amit Gabale, and Samuel Taiwo Adedokun for making the period of this study a memorable one for him and his family. Cherished is the memory of Virgil Stark who was an encourager.

The author thanks his lovely wife, Alice, for her endurance, patience, and love. What an amazing experience it has been to be blessed with his two daughters, Joy and Felicia. Without their constant support this research may not have been possible.

The author thanks the Lord for giving him inspiration through the life of his late mother, Mrs. Felicia Atinuke Onawola (nee Morohunfola), from whom he learnt the lessons of perseverance, sacrifices, and inner strength.

Style manual or journal used American Institute of Aeronautics and Astronautics Journal

Computer software used Microsoft Word

TABLE OF CONTENTS

LIST OF TABLES

LIST OF FIGURES

NOMENCLATURE

$a_1,\ a_2,\ a_n,\ A_{nm},\ A_n$	= modal amplitudes
a, b	= plate length, plate span
$A,\ B,\ D$	= extensional, coupling, bending stiffnesses
$b_3,\ b_4$	= electro-elastic coupling coefficients
$C_{ijkl}^E,\ Q_{ijkl}^E,\ [Q]^E$	= elastic constant matrix
$C_1, C_2, C_3, C_4, C_5, C_6$	= nonlinear modal amplitude terms
c_d	= aerodynamic damping term
c_{fv}	= flow speed coupling term
$c_{k3},\ c_{k4}$	= linear stiffness terms
$c_{312},\ c_{330}, c_{403}$	= nonlinear stiffness terms
$d_{ijk},\ [d]$	= piezoelectric strain coefficients
D_i	= electric displacement
e	= piezoelectric stress coefficient
$E,\ E_i, \{E\}$	= electric field
$E,\ E_s,\ E_p$	= elastic constant
$E_s,\ E_p$	= aluminum elastic constant, piezo ceramic elastic constant
f	= dielectric permittivity
h, h_p, h_s	= panel, piezo ceramic, substructure thicknesses
H	= electrical enthalpy
$H(\cdot)$	= Heaviside function
K	= kinetic energy
M_∞	= Mach number
$\{M\}$	= bending stress couple
$\{N\}$	= stress resultants
P_i	= Polarization vector
$q,\ q_a$	= dynamic pressure
$R_{31},\ R_{32}$	= moment-electric field coefficients
t	= time
T	= transpose
$u,\ v,\ w$	= displacement field along $x-,\ y-,\ z-$ directions

u^0, v^0 = midplane displacement fields
U = internal strain energy
V = workdone due to external force
w, W = deflection or transverse displacement
$w_{\max}$, $W_{\max}$ = maximum deflection
$\dot{W}$ = rate of change of deflection

x, y, z = displacement field components
δ, Δ = delta
$\delta(\cdot)$ = dirac
e_{ijk} = piezoelectric stress coefficients
ε, ε_{ij}, $[\varepsilon]$, $\{\varepsilon\}$ = strains
$\{\varepsilon^p\}$, $\{\varepsilon^0\}$ = piezoelectric strain, midplane strain
λ, λ_{cr} = dynamic pressure, critical dynamic pressure
$\{\Lambda\}$ = piezoelectric induced strain vectors
$\{\kappa\}$, κ_x, κ_y, κ_{xy} = curvature
$\kappa_{kl}^{\varepsilon}$, $[\kappa]^{\varepsilon}$, $[\kappa]^{\sigma}$ = dielectric permittivity
γ_{xy} = shear strain
τ_{xy} = shear stress
τ = nondimensional time
ρ_a = air density
ϕ, Φ = potential, airy stress potential
∇ = gradient
σ_{ij}, $[\sigma]$, $\{\sigma\}$ = elastic stress components
m_o = mass per unit area

1. INTRODUCTION

Panel flutter is the self-excited oscillation of a plate or shell when exposed to airflow along its surface [1]. This is a dynamic instability phenomenon in the supersonic/hypersonic speed regime, and is induced by the aerodynamic loads, which act only on one side of a panel. This differs from aeroelastic wing flutter, where the flow acts on both sides of the wing. Generally, flutter is an oscillatory aeroelastic instability characterized by the loss of system damping due to the presence of unsteady aerodynamic loads [2].

The consequences of aeroelastically induced motion are structural failures, and they have been observed in research aircraft, launch vehicles for spacecraft, and jet engines. The earliest reported structural failures that can be attributed to panel flutter were the failures of early German V-2 rockets during World War II [3, 4]. Panel flutter can be experienced by a vehicle that flies at a supersonic speed in the air. The skin panels experience sustained vibrations with associated limit cycle oscillations that can result in structural failures by fatigue due to the aerodynamic pressure on the vehicle surface.

Experiments indicate that there are critical dynamic pressures (air flow speeds) above which panel flutter exists. At dynamic pressures below these critical dynamic pressures the panel has random oscillations with small amplitudes. These are small compared to the panel thickness, and they die out with time. Linear structural theory predicts the critical dynamic pressure value above which the panel motion becomes

unstable and grows exponentially with time, but it only predicts the flutter boundary and the corresponding structural flutter frequency. At dynamic pressures above the critical pressure, the amplitude of vibration becomes large, and it is on the order of the panel thickness, the effect of in-plane stretching forces becomes significant and acts as a restoring force, while the aerodynamic forces tend to increase the amplitude. Therefore, the interplay of the mid-plane stretching forces, which generally restrain the motion and cause stability, and the aerodynamic forces, which grows the amplitudes and causes instability, results in the bounded limit cycle oscillations that are observed. This is shown in Fig. 1.1. Therefore linear theory becomes insufficient, and nonlinear structural theory, which is based on von Kármán large deflection plate theory, is suggested for further analysis.

Flexible structures, such as satellites, atmospheric re-entry vehicles, and other aerodynamic vehicles are generally lightly damped due to low structural damping in the materials used and the lack of other forms of damping. In these structures, vibrations have long decay times that can lead to fatigue, instability, or other problems associated with the operation of the structures. One of the earliest works of actively controlling the vibrations of these flexible structures using active materials is by Bailey and Hubbard [5] who developed an active vibration damper for a cantilever beam using a distributed-parameter actuator and distributed-parameter control theory. When these structures are made with highly distributed actuators, sensors, and processing networks [6], they are referred to as intelligent structures. The study of aeroelastic phenomena has received serious attentions in the past few decades in two particular areas of interest, namely wing flutter and panel flutter, and efforts have been made to develop controllers for these

classes of problems. Much attention has been focused in the literature on active control of wing flutter using nonlinear control techniques, but very little has been done in the area of panel flutter control using such techniques. Moon, S. H. et al. [7] noted that the system to be controlled is both nonlinear and underactuated, and that it is better to control nonlinear systems using a nonlinear control method. A nonlinear controller using a feedback linearization control method was proposed and applied to suppress panel flutter using a finite element method.

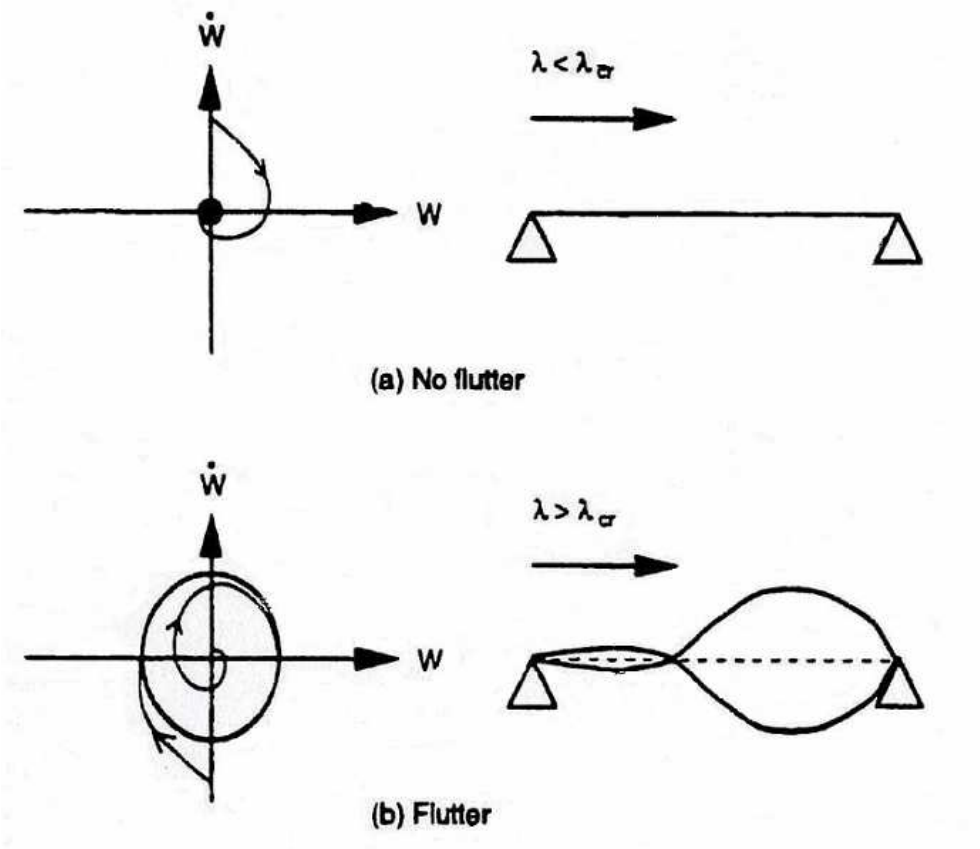

Fig. 1.1 Nonlinear oscillations of a simply-supported plate

1.1 Panel Flutter

There are voluminous works on panel flutter over several decades, with most analyses placed in one of five categories [8] based on the structural and aerodynamics theories employed, and they are described in [9 -14]. They are shown in Table 1.1. The first category is the linear structural theory and quasi-steady aerodynamic theory [9, 10]. The second is the linear structural theory and full linearized (inviscid, potential) aerodynamic theory [11, 12]. The third is the nonlinear structural theory and quasi-steady aerodynamic theory [13-18]. The fourth is the nonlinear structural theory and the full linearized (inviscid, potential) aerodynamic theory [19, 20], and the fifth is the nonlinear structural theory and the nonlinear piston aerodynamic theory [21].

The aerodynamic pressure, which acts on one side of the panel surface, is developed as a function of the panel motion. Linearized potential flow theory is recommended for air speeds close to Mach one, quasi-steady linear (first-order) piston theory is employed for supersonic air flow ($M_\infty > \sqrt{2}$), and nonlinear (third-order) piston theory is recommended for the hypersonic regime ($M_\infty > 5$). Structural theory can be linear or nonlinear depending on the order of magnitude of the transverse deflection compared to the panel thickness.

Table 1.1 Panel flutter theories

Type	Structural theory	Aerodynamic theory	Mach number
1	linear	Quasi-steady piston	$\sqrt{2} < M_\infty < 5$
2	linear	Full-linearized potential	$1 < M_\infty < 5$
3	nonlinear	Quasi-steady piston	$\sqrt{2} < M_\infty < 5$
4	nonlinear	Full-linearized potential	$1 < M_\infty < 5$
5	nonlinear	Nonlinear piston	$M_\infty > 5$

Linear panel flutter can be solved with the Fourier method in the frequency domain. The critical dynamic pressure and flutter boundary are found by increasing the aerodynamic pressure until two linear frequencies coalesce. The two values of frequencies, which are real become a complex pair. Beyond the flutter boundary, the panel will undergo fluttering motion, and the amplitude of the panel motion diverges, but various experiments indicate that the amplitude grows to a limiting value, which becomes stable, nearly sinusoidal and independent of the initial conditions. This motion is called limit cycle oscillation. This phenomenon is explained by the interplay between damping due to the structural nonlinearities and instability due to aerodynamic pressure effect. The transverse deflection of the panel is of the order of the panel thickness when it undergoes limit cycle oscillation in the fluttering zone, so linear analysis is inadequate. In order to account for the geometric nonlinearity, von Kármán large-plate theory is usually employed in nonlinear panel flutter problem, and it agrees well with experimental results [22] as shown in Fig. 1.2.

The analysis of nonlinear panel flutter involves analytical techniques such as Galerkin or the Rayleigh-Ritz method, which is used to reduce the partial differential equations of motion to a set of ordinary, nonlinear, integral-differential equations in time for the modal amplitudes. The integral terms are omitted, if quasi-steady aerodynamic theory is used instead of the linearized full (inviscid, potential) aerodynamic theory. The linear panel flutter problem can be obtained, if the nonlinear terms are omitted [23]. The set of ordinary differential equations obtained is further solved by a direct integration method, harmonic balance method, or perturbation method.

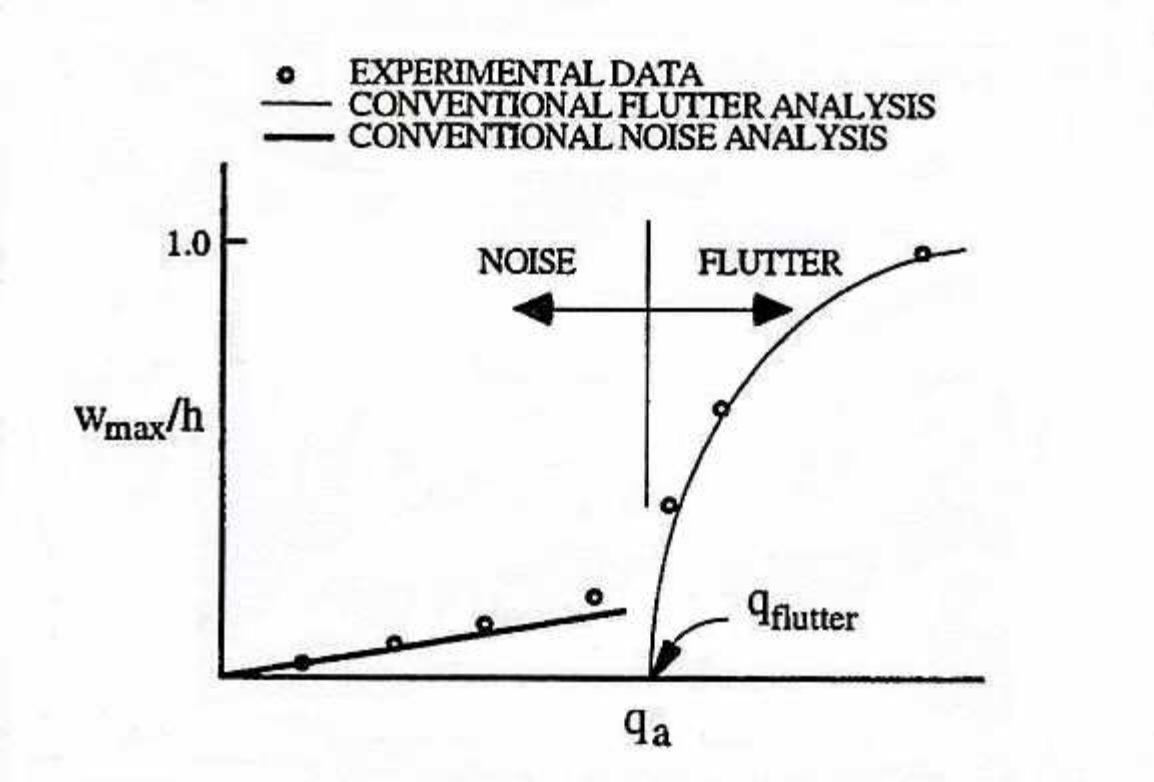

Fig. 1.2 Comparison of experimental results and first-order piston theory solutions

The numerical time integration, when employed, produces the time-displacement history, from which limit cycle oscillation is obtained.

The harmonic balance method has been widely and successfully applied to nonlinear panel analysis [1, 2, 14, 15, 17, 18, 21, 25, 26]. Using this method, Fung [2, 14] and Kobayashi [17] solved 2-D plates, and Librescu [18] developed general solutions for rectangular and cylindrical specific orthotropic plates. Eastep and McIntosh in [21] used a Rayleigh-Ritz approximation to Hamilton's variational principle instead of Galerkin's method to set up the equations of motion in the spatial domain for the solved rectangular plates. Kuo, Morino and Dugundji [1] also solved the nonlinear panel flutter problem for rectangular plates. Eslami [25] studied specific orthotropic panels. Yen and

Lau [26] studied the dynamical behaviour of a hinged-hinged 2-D plate excited by supersonic flow.

Perturbation methods are used to solve problems with small nonlinearity due to the assumption of small disturbance from an equilibrium position, and they have been used to solve panel flutter for rectangular plates by Morino [1, 27], and by Eslami [25] for specific orthotropic plates.

The nonlinear theory of supersonic panel flutter is deterministic. Ibrahim and Orono [28] investigated stochastic nonlinear flutter of a simply-supported 2-D isotropic panel subjected to random in-plane forces. The aerodynamic loading was modeled using a first-order quasi-steady piston theory. A general moment equation for two- and three-mode interactions was derived by using the Fokker-Planck equation approach. The stochastic nonlinear flutter was studied using Gaussian and first-order non-Gaussian closure schemes. They concluded that the nonlinear random flutter of panels in terms of four and more modes can adequately be determined by using the Gaussian closure scheme.

The other alternative approaches to Galerkin's method and modal expansion are numerical methods (finite difference and finite element representations) and separation of variables or so-called exact solutions. The former is particularly useful in solving nonlinear panel flutter problems without simple boundary conditions or problems with equations of motion with various terms which makes the analytical solution improbable. Survey of various applications of finite element methods to nonlinear panel flutter can be found in Han and Yang [29] up to 1983, Gray and Mei [8] up to 1991, Zhou et al. [30] up to 1994.

1.2 Intelligent Structures

Pierre and Jacques Curie [31] discovered that some crystals produce charges on their surfaces when compressed in particular directions, and those charges are proportional to the applied pressure. These charges are withdrawn when the applied pressure is removed. It was also found that these crystals become strained when they are electrically polarized. This effect is called piezoelectricity, and it is exhibited by crystalline materials, such as quartz and rochelle salt.

Nowadays, the most commonly used piezoelectric materials include ceramics called lead zirconate titanate (PZT), and polymers such as poly-vinylidene fluoride (PVDF), Macro Fiber Composites (MFC) and Active Fiber Composites (AFC).

Piezoelectric materials act as a generator by converting mechanical energy into electrical energy when pressure is applied, and this is known as the sensor mode or the direct effect. Conversely, it acts as motor by converting electrical energy into mechanical energy, when electric field is applied to it, and this is known as the actuator mode or converse effect. It also acts as a capacitor for storing electrical energy. These materials have been used extensively in electromechanical transducers, such as ultrasonic generators, filters, strain gages, pressure transducers, accelerometers, sensors, and actuators because of their direct and converse effects.

Piezoelectric layers or patches are usually bonded to or embedded in the surface of a structure. The mechanical/electrical behavior of these flexible structure members can then be monitored or modified by the piezoelectric layers or patches used as sensors or actuators.

Actuation strain is the component of strain that is due to stimuli other than mechanical stress, and it can be produced by piezoelectric materials. This strain physically causes induced strains to be produced. The potential applications for induced strain actuators are their uses as highly distributed actuators in intelligent structures. Therefore, flexible structures can be controlled by the use of smart sensors and actuators. Intelligent structures having distributed actuators with induced strain actuations can be used to design structures with intrinsic vibration and shape control capabilities. Some studies have been carried out on induced strain actuation for beams [6, 32, 33, 34, 35] and plates [36, 37]. The actuation strain is modeled into the constitutive relations as is usually done with thermal strain. In [6], both static and dynamic models were developed for segmented piezoelectric and substructure couplings. These were incorporated into the Bernoulli-Euler beam equations, and these models were refined into three types [32]: the uniform strain model with only extensional strain in the actuator for surface bonded actuators; the Bernoulli-Euler or consistent strain model, which accounts for both extension and bending in the actuator and is applicable to both surface bonded or embedded actuators; and finite element models which account for extension, bending and shear in the actuator and structure. Experimental results were used to validate the beam actuation models presented.

The static model of the mechanical coupling of the segmented piezoelectric actuators accounts for only pure bending of the elastic substructure, therefore Im and Atluri [34] proposed a refined model, which includes the transverse shear forces, axial forces and the bending moments induced by actuators.

Crawley and Lazarus [36] formulated a general model of the induced strain actuation of plates with various boundary conditions and externally applied loads for both isotropic and anisotropic plates that are entirely or partially covered with piezoelectric actuators in various orientations, either bonded to or embedded in the substrates. This model combines both the actuators and the substrates into one integrated structure, and it is referred to as the "consistent plate model." This model considers the induced strain actuators to be plies of a laminated plate. There is an assumption of consistent deformations in the actuators and the substrates. The strain distribution is assumed to result from a linear combination of in-plane extensional (constant strain through the thickness) and bending (linearly varying through the thickness) displacements.

Hagood, Chung and von Flotow [38] modeled the effects of dynamic coupling between a structure and an electrical network through the piezoelectric effect. Burke and Hubbard [39, 40] applied a spatially shaped distributed actuator for the vibration control of a simply supported beam, and this distribution facilitates the control of desired vibrational modes.

Static and dynamic models have been derived for segmented piezoelectric actuators that are bonded to elastic substructures or embedded in laminated structures [6]. These models are used to predict the response of a structural member to a command voltage applied to the actuators and give guidance as to the optimal locations for their placements.

Dimitriadis, Fuller and Rogers [41] extended the static and dynamic models developed in [6] for piezoelectric elements bonded to and embedded in one dimensional beams to two dimensional plates by estimating the load induced by the actuators to the

supporting elastic structures. The results were used to selectively excite and suppress particular vibrational modes leading to improved control behavior.

A conservation of strain energy model has been used to determine the equivalent force and moment induced by finite-length spatially-distributed induced strain actuation attached to or embedded in laminate beams and plates using the applied moment on the cross-section of the edges of the actuators [35]. This model was extended into developing classical laminated plate theory (CLPT) for a laminate plate with induced strain actuators for actuator patches that are spatially distributed [37].

This “consistent plate model” has been experimentally verified and has been shown to be the most accurate representation of the actual behavior of both discrete surface bonded or embedded actuators, either segmented or continuous.

The placement of actuators primarily is dependent on the mode to be controlled. The placement of piezoelectric actuators for controlling particular free vibration modes was considered by Crawley and de Luis [6]. Lee [42, 43] developed a piezoelectric laminate theory based on modal sensors and actuators. These modal sensors/actuators sense and actuate the modal coordinate of a particular mode of a beam or plate. They are also used to excite or measure combinations of modes. Tanaka [44] placed a number of sensor patches on a structure to measure the response of a number of modes. Results demonstrate that modes can be selectively excited and that the geometry of the actuator shape affects the distribution of the response among modes [41 – 44].

A piezoelectric material can be used as an actuator or a sensor, but when it is made to simultaneously effect deformations and sense the strain in structural members, thereby combining both functions in a single device, then it is referred to as a “self-sensing

piezoelectric actuator," or simply "simultaneous sensor actuator" (SSA), and Anderson and Hagood [45], and Anderson, Hagood and Goodliffe [46] presented a coupled electromechanical model for such a SSA. They also investigated issues relating to its implementation in both open and closed-loop experiments performed on a cantilevered beam. Typically, the current drawn by the piezoelectric material is ignored when it is used as an actuator. When the current drawn is taken into account, there is the possibility of reconstructing the actuator strain from a voltage-driven piezoelectric. Dosch, Inman and Garcia [47] developed a technique for using a self-sensing actuator in a closed-loop that is truly collocated and effective in vibration suppression of intelligent structures.

In the past few decades, a tremendous amount of research has been devoted to the vibration control of structures. While passive control improves the performance characteristics of a structure through the use of materials or devices that enhance the damping and/or stiffness characteristics of the structure, active control achieves the desirable performance characteristics through feedback control, whereby actuators apply forces or moments to a structure based on the structural response measured by the sensors.

Some of the research in the field of vibration control of flexible structures using piezoelectric sensors and actuators include efforts by Plump and Hubbard, Sung and Chen, Chen et. al., Joseph [48 - 51]. They studied structures that are able to sense and control their own behaviors, so as to achieve much higher levels of operational performance than conventional materials and structures. A technique called positive position feedback (PPF) for vibration suppression in large space structures was also investigated, and this technique makes use of generalized displacement measurements.

These works also include suppression of elastodynamic responses of high-speed flexible linkage mechanisms by employing a state feedback optimal control scheme. Piezoceramics are used to generate the control inputs, and they are also used as sensing devices.

1.3 Panel Flutter Suppression

The effectiveness of using passive or active control of flexible structures has been demonstrated by many researchers. However, in the area of panel flutter suppression using piezoelectric materials, only a few research efforts have been reported [52 - 57]. Frampton, et. al. [57] investigated the active control of panel flutter with piezoelectric transducers by implementing direct rate feedback control, and they demonstrated a significant increase in the flutter boundaries.

Chuh Mei and his research group [54, 56, 58 - 60] have carried out extensive research on the suppression of nonlinear panel flutter using piezoelectric actuators. They used both the finite element method and Galerkin's method with modal expansion. The finite element models account for nonlinear stiffness matrices, thermal and aerodynamic loads on the panel. Optimal control was used to actively suppress large-amplitude, limit cycle flutter motions of rectangular plates at supersonic speeds using piezoelectric actuators.

Moon. S. H. et al. [61, 62] investigated both active and passive suppression schemes for nonlinear flutter of composite panel. Optimal controllers based on linear optimal control theory were designed for active suppression schemes, while piezoelectric

actuators connected with an inductor-resistor series shunt circuits were used for the passive suppression. An active/passive hybrid piezoelectric network was also formulated.

Since the previous studies on panel flutter suppression used optimal controllers for linearized models, Moon, S. H. et al. [5] applied a nonlinear controller using a feedback linearization control method to suppress panel flutter using the finite element method. This technique was also employed in developing nonlinear control techniques for a prototypical wing sections with torsional nonlinearies at Texas A. & M. [63]. Locally asymptotically stable (nonlinear) feedback controllers for a range of flow speeds and elastic axis locations were derived for this aeroelastic system using partial feedback linearization techniques when either the pitch or plunge is chosen as the output. This leads to a partial input-output feedback linearizing coordinate transformation with the use of a single trailing-edge control surface. As a result, the associated zero dynamics of the subsystem was studied, and it was found that it can also be locally asymptotically stable. Full feedback linearization was also carried out with two trailing-edge control surfaces. When the nonlinear partial feedback linearization is constructed so as to explicitly control the pitch degree of freedom, the zero dynamics of the closed-loop system are linear. But, when the nonlinear partial feedback linearization explicitly controls the plunge degree of freedom, closed-loop stability of the zero dynamics is considerably more difficult. It is shown that there exist locations of the elastic axis and speeds of the subsonic/incompressible flow for which feedback strategy exhibits a wide range of bifurcational phenomena.

1.4 Objectives and Scope

There is much research going on in the development of intelligent systems using active materials, and some of these efforts include the development of intelligent plates. Panel flutter has also posed tremendous challenges to aeroelasticians, and has generated lots of research in the design of structural surfaces exposed to aerodynamic loads, especially in supersonic environments. The application of these intelligent plates in aircraft or vehicles and surfaces in a fluid medium has the potential of making these surfaces actively respond to external stimuli. These intelligent plates have actuators and sensors embedded or bonded to their surfaces, and they are connected to processors which modify the signals so that these intelligent plates are able to react to stimuli that can cause large deflections and instability resulting in the failure of the panel. With these developments, advanced aircraft or vehicles and surfaces in a fluid medium can operate in harsh environments.

The main objective of this research is to investigate a technique for suppressing the fluttering of a fluid loaded flat panel or flat panel with aerodynamic loads, which is also acted upon by in-plane forces. This problem is also widely known as panel flutter suppression. The technique that is used is based on nonlinear control theory. The main idea is to transform the nonlinear panel flutter problem into an equivalent controllable linear problem that can be written in simple Brunovsky canonical form by the method called feedback linearization. This involves developing nonlinear feedback control laws, which cancel the nonlinear dynamics resulting in a linear system, and a pole placement

technique is then employed so as to make the states of the linearized feedback models locally asymptotically stable at a given equilibrium.

The active materials used in this investigation are piezoelectric ceramics, and they have dual effects coupling their electrical and structural properties. The electromechanical quantities involved are presented in Chapter 2 and these lead to linear piezoelectric constitutive relations.

Equations of motion are given for a flat panel with bonded and distributed actuators and sensors subject to aerodynamic loads, in-plane loads and applied electric fields. These equations are coupled nonlinear partial differential equations, which are reduced to nonlinear ordinary differential equations in time, and presented in state-space format, in Chapter 3.

In Chapter 4, feedback linearizing controllers are developed for a fluid loaded flat panel with limit cycle oscillations at a dynamic pressure above the critical dynamic pressure with or without externally applied in-plane loads. The suppression of the oscillations after the onset of flutter is investigated. Numerical simulations are carried out in Chapter 5 to study the feedback linearized methodologies, and to establish the stability of the resulting states. The conclusions to this investigation are presented in Chapter 6.

2. PIEZOELECTRICITY

Piezoelectric materials are active materials that are either ceramic or polymeric. Ceramic materials include lead zirconante titanates (PZT) and single crystals; while polymeric materials include polyvinylidene fluoride (PVDF), macro fiber composite (MFC) and Active Fibers (AFC). These materials are bonded to the surface of, or embedded into flexible structural members, so that actuation and sensing are achieved at the material level.

2.1 Characteristics of the Materials

A ceramic material is made active by a poling process, which is the application of a large external electrical field, which aligns the randomly orientated unit cells in the medium. One can consider a material with geometrical orientation as shown in Fig. (2.1).

The coupling coefficients are defined by the direction of the poling. Three mutually perpendicular directions are shown along the axes 1, 2 and 3. There are also three other modes, and these are 4, 5, and 6, which represent shear in the 1, 2 and 3 directions, respectively. The material, is poled as shown, in the 3-direction, so that the polarization is taken to be along that direction. The piezoelectric strain coefficient, piezoelectric stress coefficient, and permittivity are represented as d, e, and κ, respectively. They have 2 subscripts. The first indicates the direction of the electric field, while the second indicates the direction of strain. Therefore, the piezoelectric coefficients are d_{31}, d_{32}, d_{33}, d_{15}, d_{25},

and d_{36}. The most commonly used coefficient is d_{31}, and this implies that electric field is applied in the direction of polarization, 3-direction, while, the induced strain is in the 1-direction.

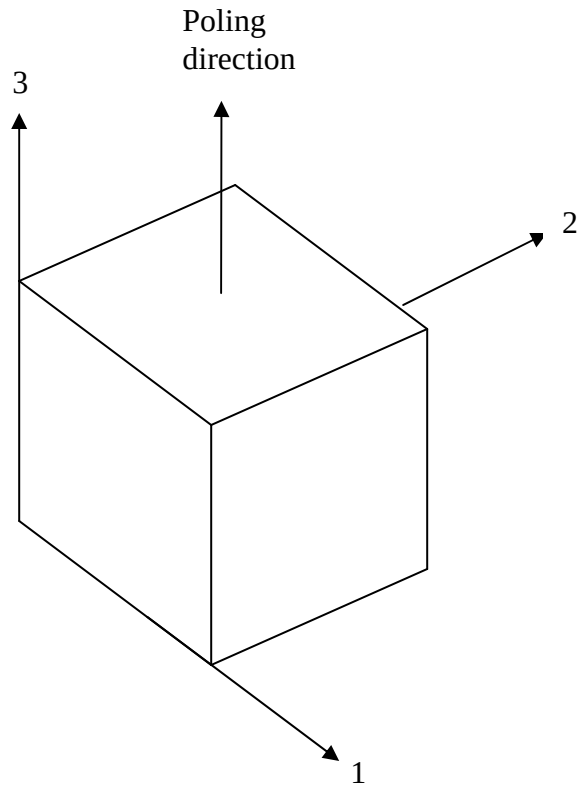

Fig.2.1 Geometrical orientation of an active material showing the poling direction

Piezoelectric materials have distinctive effects. They develop an electrical charge when subjected to mechanical stress in the direct piezoelectric effect, and conversely they develop mechanical strain when subjected to an electrical field. Therefore, they can convert electrical energy into mechanical energy and vice-versa. The applied electric potential produces an electrical field across the material that induces mechanical strain in it, while in reversal; the application of stress to the same material generates electrical charges on it.

The direct piezoelectric effect is the production of both positive and negative electric charges on the corresponding surfaces, and it results in the deformation that takes place under external pressure (stress). Thus, there is polarization of the medium due to deformation in the absence of an electric field, E_i, and the relationship between the polarization vector, P_i, is given as

$$P_i = e_{ijk}\varepsilon_{jk} \text{ or } P_i = d_{ijk}\sigma_{jk} \tag{2.1}$$

The converse piezoelectric effect is the mechanical deformation which results from the application of electric field, E_i, due to the polarization of a medium, and the relationship is given as

$$\varepsilon_{jk} = d_{ijk}E_i \tag{2.2}$$

Therefore, there is strong coupling between the deformation fields and internal electric fields.

2.2 Electrical Enthalpy and Electric Field

The electrical enthalpy H describes the amount of energy stored in a material and is defined in [64]. The electrical enthalpy can be written as

$$H = U - E_i D_i \tag{2.3}$$

where U is the total internal energy, E and D are the electric field and displacement vectors, respectively.

Toupin[65] formulated electric enthalpy density using a polynomial approximation based on a power series expansion about the natural state of a piezoelectric medium. The result is as shown

$$H = H(\varepsilon, E) \tag{2.4}$$

where, ε is strain, and E is the electric field.

$$H = \tfrac{1}{2} C^{E}{}_{ijkl} \varepsilon_{ij} \varepsilon_{kl} - e_{ijk} E_i \varepsilon_{jk} - \tfrac{1}{2} \kappa^{\varepsilon}_{kl} E_k E_l \tag{2.5}$$

$$H = \tfrac{1}{2} \{\varepsilon\}^T [Q]^E \{\varepsilon\} - \{E\}^T [e] \{\varepsilon\} - \tfrac{1}{2} \{E\}^T [\kappa]^{\varepsilon} \{E\} \tag{2.6}$$

where, C^{E}_{ijkl} is used interchangeably with Q, and C^{E}_{ijkl}, e_{ijk}, and $\kappa^{\varepsilon}_{ij}$ are elastic stiffness constants, piezoelectric stress constant, and dielectric permittivity, respectively.

The electric field vector is the negative gradient of the electric potential, ϕ, and it is assumed to vary linearly in the thickness, t_k, direction, that is,

$$E = -\nabla \phi \tag{2.7}$$

$$= \{0 \quad 0 \quad E_z\}^T$$

with $E_z = -\frac{\phi}{t_k}$

2.3 Linear Piezoelectric Constitutive Relations

Although there are many nonlinear phenomena in piezoelectric materials, linear constitutive relations are often used to describe the behavior of piezoelectric layers. The mechanical stress and strain vectors, σ and ε, respectively, are related through the electric enthalpy H. The linear piezoelectric constitutive equations obtained from [66] are given in Eq. (2.8) and Eq. (2.9).

$$\sigma_{ij} = \frac{\partial H}{\partial \varepsilon_{ij}} = C^{E}{}_{ijkl}\varepsilon_{kl} - e_{kij}E_k \tag{2.8}$$

$$D_i = -\frac{\partial H}{\partial E_i} = e_{ikl}\varepsilon_{kl} + \kappa^{\varepsilon}_{ik}E_k \tag{2.9}$$

and, in matrix form

$$\{\sigma\} = \left[\overline{Q}\right]^{E}\{\varepsilon\} - [e]^{T}\{E\} \tag{2.10}$$

$$D = [e]\{\varepsilon\} + [\kappa]^{\varepsilon}[E] \tag{2.11}$$

Just as in the relationship between mechanical stress and mechanical strain, the piezoelectric stress coefficient is proportional to the piezoelectric strain coefficient, with elastic material properties as the constants of proportionality. Hence,

$$[e] = [d]\left[\overline{Q}\right]^{E} \tag{2.12}$$

substituting Eq. (2.12) into Eq. (2.8), one obatins

$$\{\sigma\} = \left[\overline{Q}\right]^{E}\left(\{\varepsilon\} - [d]^{T}\{E\}\right) \tag{2.13}$$

We can write

$$\begin{aligned}[\sigma] &= [Q]^{E}\{\varepsilon\} - \left([d][Q]^{E}\right)^{T}\{E\} \\ &= [Q]^{E}\left(\{\varepsilon\} - [d]^{T}\{E\}\right)\end{aligned} \tag{2.14}$$

One can observe that the piezoelectric induced strain is the product of the applied electric field and piezoelectric strain coefficient of the material, and it is written as

$$\{\Lambda\} = [d]^T \{E\} \tag{2.15}$$

The free permittivity matrix $[\kappa]^{\varepsilon}$ is easier to obtain than the clamped permittivity matrix $[\kappa]^{\sigma}$, We can use the relationship below to relate the two.

$$[\kappa]^{\varepsilon} = [\kappa]^{\sigma} - [d][Q]^E [d]^T \tag{2.16}$$

Similarly, one can re-write the expression for the electrical displacement density using Eq. (2.11), Eq. (2.12), and Eq. (2.16) as

$$\begin{aligned} \{D\} &= [d][Q]^E \{\varepsilon\} + \left([\kappa]^{\sigma} - [d][Q]^E [d]^T\right)\{E\} \\ &= [d][Q]^E \left(\{\varepsilon\} - [d]^T \{E\}\right) + [\kappa]^{\sigma} \{E\} \end{aligned} \tag{2.17}$$

In this section, both the linear piezoelectric constitutive relations and linear electrical displacement density relations have been obtained. They are given by

$$\begin{Bmatrix} \sigma_{xx} \\ \sigma_{yy} \\ \tau_{xy} \end{Bmatrix}_k = \begin{bmatrix} 1 & \nu & 0 \\ \nu & 1 & 0 \\ 0 & 0 & \frac{1}{2}(1-\nu) \end{bmatrix}_k \left(\begin{Bmatrix} \varepsilon_{xx} \\ \varepsilon_{yy} \\ \gamma_{xy} \end{Bmatrix}_k - E_{ik} \begin{Bmatrix} d_{xx} \\ d_{yy} \\ d_{xy} \end{Bmatrix}_k \right) \tag{2.18}$$

and

$$D_i^{(k)} = \begin{Bmatrix} d_{xx} & d_{yy} & d_{xy} \end{Bmatrix}^{(k)} \begin{bmatrix} 1 & \nu & 0 \\ \nu & 1 & 0 \\ 0 & 0 & \frac{1}{2}(1-\nu) \end{bmatrix}^{(k)} \left(\begin{Bmatrix} \varepsilon_{xx} \\ \varepsilon_{yy} \\ \gamma_{xy} \end{Bmatrix} - E_i^{(k)} \begin{Bmatrix} d_{xx} \\ d_{yy} \\ d_{xy} \end{Bmatrix}^{(k)} \right) + \kappa_{iik}^{\sigma} E_i^{(k)} \tag{2.19}$$

respectively.

3. FORMULATIONS

In this chapter, the generalized nonlinear dynamic equations for a simply supported rectangular panel with piezoelectric layers are presented.

The flat plate or panel is considered to be an intelligent plate, and it is made up of the host substructure and piezoelectric materials embedded within the host or bonded to the surface of the host. The panel considered in this study is thin. The piezoelectric materials are in the form of distributed patches or continuous layers, while the host substructure is considered to be an isotropic material.

Many research efforts have been conducted in the field of vibration control of structures using piezoelectric actuators and sensors. In the case studied here, the structure is a simply supported rectangular intelligent plate or panel, and its generalized nonlinear dynamic equations are derived as in [54]. The intelligent plate is considered to undergo large transverse displacement of the order of the plate thickness, therefore, von Kárman large-deflection plate theory, which accounts for the structure nonlinearity, is used for modeling the plate deflection. The linear piezoelectric theory is used to derive the equations of piezoelectric actuation and sensing, and first-order piston theory or the quasi-steady supersonic theory is used to model the aerodynamic force due to the supersonic fluid flow.

3.1 Aerodynamic Forces

In the case where the fluid flow over a panel is considered as aerodynamic loads or forces, this problem is sometimes referred to as panel flutter, in the literature. The aerodynamics pressures can be represented by quasi-steady first-order piston theory, full linearized (inviscid, potential) aerodynamic theory, or nonlinear piston aerodynamic theory. The aerodynamic theory that is applied in this study is the quasi-steady first-order piston aerodynamic theory, and it is employed to model the aerodynamic pressure when a flight vehicle is in the supersonic airflow regime. This theory describes the aerodynamic loads on a skin panel as pressure on a piston in a long narrow tube with a given velocity, and this is expressed as in [24].

$$\Delta p = -\frac{2q_a}{\beta}\left[\frac{\partial w}{\partial x} + \frac{M_\infty^2 - 2}{M_\infty^2 - 1}\frac{1}{V_\infty}\frac{\partial w}{\partial t}\right] \tag{3.1}$$

where $q_a = \frac{1}{2}\rho_a V_\infty^2$ is the dynamic pressure, ρ_a is the air density, V_∞ the free stream airflow speed, M_∞ the Mach number, w the transverse displacement of the panel, and $\beta = \sqrt{M_\infty^2 - 1}$.

3.2 Displacement Field Theory:

The displacement field theory is based on Kirchhoff's hypothesis, and it states that line elements which originally are perpendicular to the middle surface of the plate remain straight and normal to the deformed middle surface, and there is no change in length. The displacement field, which comprises longitudinal u, and normal displacements v, in the plane of the plate, and transverse displacement w, can be written as

$$u = u_0(x, y, t) - zw_{0,x}$$

$$v = v_0(x, y, t) - zw_{0,y}$$

$$w = w_0(x, y, t) \qquad \text{(3.2a,b,c)}$$

3.3 Nonlinear Strain-Displacement Relations:

In panel flutter, the plate displacement can be of the order of the thickness of the plate due to both static and dynamic instabilities and the associated limit cycle. Therefore, the plate is considered to undergo large displacement, and one can use von Kármán's theory, which considers nonlinear strain-displacement relations.

$$\varepsilon_{xx}^0 = \frac{\partial u^0}{\partial x} + \frac{1}{2}\left(\frac{\partial w}{\partial x}\right)^2$$

$$\varepsilon_{yy}^0 = \frac{\partial v^0}{\partial y} + \frac{1}{2}\left(\frac{\partial w}{\partial y}\right)^2$$

$$\gamma_{xy}^0 = \frac{\partial u^0}{\partial y} + \frac{\partial v^0}{\partial x} + \frac{\partial w}{\partial x}\frac{\partial w}{\partial y} \qquad \text{(3.3a,b,c)}$$

The flat panel is considered to be an isotropic material, and it is thin, so that the ratio of the length or width over thickness of the panel is greater than 20. The rotary inertia and transverse shear deformation effects are negligible, hence from the assumptions of Kirchhoff's hypothesis, the transverse strain components ε_{zz}, ε_{xz} and γ_{yz} are taken to be negligible, so that, one can write

$$\varepsilon_{zz} = \frac{\partial w}{\partial z} = 0$$

$$\gamma_{xz} = \frac{\partial u}{\partial z} + \frac{\partial w}{\partial x} = 0$$

$$\gamma_{yz} = \frac{\partial v}{\partial z} + \frac{\partial w}{\partial y} = 0 \qquad \text{(3.4a,b,c)}$$

and from von Kármán's strain-displacement relations, one obtains

$$\varepsilon_{xx} = \frac{\partial u^0}{\partial x} + \frac{1}{2}\left(\frac{\partial w}{\partial x}\right)^2 - z\frac{\partial^2 w}{\partial x^2}$$

$$\varepsilon_{yy} = \frac{\partial v^0}{\partial y} + \frac{1}{2}\left(\frac{\partial w}{\partial y}\right)^2 - z\frac{\partial^2 w}{\partial y^2}$$

$$\gamma_{xy} = \frac{1}{2}\left(\frac{\partial u^0}{\partial y} + \frac{\partial v^0}{\partial x} + \frac{\partial w}{\partial x}\frac{\partial w}{\partial y}\right) - z\frac{\partial^2 w}{\partial x \partial y}$$

In vector form

$$\{\varepsilon\} = \begin{Bmatrix} \varepsilon_{xx} \\ \varepsilon_{yy} \\ \gamma_{xy} \end{Bmatrix} = \begin{Bmatrix} \dfrac{\partial u^0}{\partial x} + \dfrac{1}{2}\left(\dfrac{\partial w}{\partial x}\right)^2 - z\dfrac{\partial^2 w}{\partial x^2} \\ \dfrac{\partial v^0}{\partial y} + \dfrac{1}{2}\left(\dfrac{\partial w}{\partial y}\right)^2 - z\dfrac{\partial^2 w}{\partial y^2} \\ \dfrac{1}{2}\left(\dfrac{\partial u^0}{\partial y} + \dfrac{\partial v^0}{\partial x} + \dfrac{\partial w}{\partial x}\dfrac{\partial w}{\partial y}\right) - 2z\dfrac{\partial^2 w}{\partial x \partial y} \end{Bmatrix} \qquad \text{(3.5.)}$$

that is

$$\begin{Bmatrix} \varepsilon_{xx} \\ \varepsilon_{yy} \\ \gamma_{xy} \end{Bmatrix} = \begin{Bmatrix} \varepsilon^0_{xx} \\ \varepsilon^0_{yy} \\ \gamma^0_{xy} \end{Bmatrix} + z\begin{Bmatrix} \kappa_x \\ \kappa_y \\ \kappa_{xy} \end{Bmatrix}$$

where, the middle-surface strain components are

$$\{\varepsilon^0\} = \begin{Bmatrix} \varepsilon_{xx}^0 \\ \varepsilon_{yy}^0 \\ \gamma_{xy}^0 \end{Bmatrix} = \begin{Bmatrix} \dfrac{\partial u^0}{\partial x} + \dfrac{1}{2}\left(\dfrac{\partial w}{\partial x}\right)^2 \\ \dfrac{\partial v^0}{\partial y} + \dfrac{1}{2}\left(\dfrac{\partial w}{\partial y}\right)^2 \\ \dfrac{1}{2}\left(\dfrac{\partial u^0}{\partial y} + \dfrac{\partial v^0}{\partial x} + \dfrac{\partial w}{\partial x}\dfrac{\partial w}{\partial y}\right) \end{Bmatrix} \tag{3.6}$$

and the curvatures are given by

$$\{\kappa\} = \begin{Bmatrix} \kappa_x \\ \kappa_y \\ \kappa_{xy} \end{Bmatrix} = \begin{Bmatrix} -\dfrac{\partial^2 w}{\partial x^2} \\ -\dfrac{\partial^2 w}{\partial y^2} \\ -2\dfrac{\partial^2 w}{\partial x \partial y} \end{Bmatrix} \tag{3.7}$$

or, simply

$$\{\varepsilon\} = \{\varepsilon_m^0\} + \{\varepsilon_\theta^0\} - z\{\kappa\}$$

$$\{\varepsilon\} = \{\varepsilon^0\} - z\{\kappa\}$$

3.4 Constitutive Equations

In the analysis carried out in this study, both the elastic and the piezoelectric properties of the piezoelectric ceramic utilized are included. The stress-strain relations for an active/piezoelectric layer in an intelligent structure are given by the linear piezoelectric constitutive equations obtained in Eq. (2.18), that is,

$$\{\sigma\} = [\overline{Q}]_p \left(\{\varepsilon^0\} - z\{\kappa\} - \{\varepsilon^p\}\right)$$

$$\begin{Bmatrix} \sigma_{xx} \\ \sigma_{yy} \\ \tau_{xy} \end{Bmatrix} = \frac{E_p}{1-\nu_p^2} \begin{bmatrix} 1 & \nu_p & 0 \\ \nu_p & 1 & 0 \\ 0 & 0 & \frac{1}{2}(1-\nu_p) \end{bmatrix} \left(\begin{Bmatrix} \varepsilon_{xx} \\ \varepsilon_{yy} \\ \gamma_{xy} \end{Bmatrix} - e_3 \begin{Bmatrix} d_{31} \\ d_{32} \\ d_{36} \end{Bmatrix} \right) \tag{3.8a}$$

It can easily be observed that when any layer is passive or the piezoelectric properties of an active/piezoelectric layer is not activated, the stress-strain relations are given in Eq. (3.8b). This is simply achieved by taking the electric field term to be zero in the linear piezoelectric constitutive equations derived, and they are the same as in the literatures for purely passive layers.

$$\{\sigma\} = \left[\overline{Q}\right]_s \left(\{\varepsilon^0\} - z\{\kappa\}\right)$$

$$\begin{Bmatrix} \sigma_{xx} \\ \sigma_{yy} \\ \tau_{xy} \end{Bmatrix} = \frac{E_s}{1-\nu_s^2} \begin{bmatrix} 1 & \nu_s & 0 \\ \nu_s & 1 & 0 \\ 0 & 0 & \frac{1}{2}(1-\nu_s) \end{bmatrix} \begin{Bmatrix} \varepsilon_{xx} \\ \varepsilon_{yy} \\ \gamma_{xy} \end{Bmatrix} \tag{3.8b}$$

3.5 Dynamic Version of the Principle of Virtual Work

The equations of motion are derived using the dynamic version of the principle of virtual work or Hamilton's principle. The derivation accounts for both the elastic work done and piezoelectric effect.

$$\int_0^t \left(\delta U + \delta V - \delta K - \delta W_e\right) dt = 0 \tag{3.9}$$

where δK and δU are the virtual kinetic energy and virtual internal strain energy of the system, δW_e is the virtual electrical energy, and δV is the virtual work done due to external forces and the applied surface charge only.

The virtual internal strain energy δU is given as:

$$\delta U = \int_{\Omega_0} \int_{-\frac{h}{2}}^{\frac{h}{2}} \left(\sigma_{xx}\delta\varepsilon_{xx} + \sigma_{yy}\delta\varepsilon_{yy} + 2\sigma_{xy}\delta\varepsilon_{xy}\right) dz dx dy \tag{3.10a}$$

The virtual external applied load δV is given as:

$$\delta V = -\int_{\Omega_0} (\Delta p_s + \Delta p_a)\delta w dx dy \tag{3.10b}$$

where Δp_s = static pressure differential on the surface of the plate, excluding aerodynamic loading, and Δp_a is the aerodynamic loading over the surface of the plate.

The virtual kinetic energy δK is given as:

$$\delta K = \int_{\Omega_0} m_o \frac{\partial w}{\partial t} \delta\left(\frac{\partial w}{\partial t}\right) dx dy \tag{3.10c}$$

The variational quantities obtained in Eq. (3.10) are substituted into Eq. (3.9), and after carrying out the appropriate integration across the plate thickness, quantities such as the stress resultants and bending couples can be obtained. After carrying out the integration by parts and applying appropriate variational statements, these become the von Kármán equations for a plate with large deflections, with the piezoelectric terms included. Reference can be made to [13, 54, 67] where appropriate derivations were carried out.

3.6 Stress Resultants and Bending Couples

Stress resultants, N, and bending couples, M, are the forces and couples per unit width, and they are defined as

$$\left(\{N\}, \{M\}\right) = \int_{-\frac{h}{2}}^{\frac{h}{2}} \{\sigma\}_k (1, z) dz \tag{3.11}$$

Substituting Eq. (3.8) into the above equations result in the constitutive relations for the laminated panel used as an intelligent plate with piezoelectric ceramics bonded to both surfaces of the host layer. The stress components in the plate are integrated over each

layer thickness, and thereafter the stress resultants in each layer are summed for the whole plate. Therefore, the stress resultants and bending couples are given by

$$\begin{Bmatrix} N \\ M \end{Bmatrix} = \begin{bmatrix} A & B \\ B & D \end{bmatrix} \begin{Bmatrix} \varepsilon^0 \\ \kappa \end{Bmatrix} - \begin{Bmatrix} N^p \\ M^p \end{Bmatrix} \tag{3.12}$$

where N^p and M^p are the piezoelectric induced inplane forces and bending moments. The stiffness terms are the extensional stiffness matrix, $[A]$, bending stiffness matrix, $[D]$, and coupling (stretching-bending) stiffness matrix, $[B]$; and these are represented as

$$([A],[B],[D]) = \int_{-\frac{h}{2}}^{\frac{h}{2}} \{\sigma\}_k \left(1, z, z^2\right) dz \tag{3.13}$$

The piezoelectric layers are assumed to be symmetrically bonded to the host layer, therefore the laminate does not exhibit coupling between bending and stretching, hence the coupling matrix, $[B] = 0$. Generally, we consider that the Poisson ratio for both host and piezoelectric materials are similar, hence $v_s = v_p = v$. The stiffness matrices are represented as

$$[A] = \frac{Eh}{1-v^2} \begin{bmatrix} 1 & v & 0 \\ v & 1 & 0 \\ 0 & 0 & \frac{1}{2}(1-v) \end{bmatrix} \tag{3.14a}$$

$$[D] = D \begin{bmatrix} 1 & v & 0 \\ v & 1 & 0 \\ 0 & 0 & \frac{1}{2}(1-v) \end{bmatrix} \tag{3.14b}$$

with the equivalent panel elastic constant,

$$E = \frac{1}{h}\left(E_s h_s + E_p (h - h_s)\right) \tag{3.15a}$$

and equivalent panel bending stiffness

$$D = \frac{1}{12(1-\nu^2)}\left(E_s h_s^3 + E_p(h^3 - h_s^3)\right) \tag{3.15b}$$

3.7 Piezoelectric In-plane Force and Moment

The piezoelectric materials are assumed to be perfectly bonded to the entire top and bottom of the panel surfaces; so that classical analytical approaches can be applied to the problem of panel flutter in this research.

The piezoelectric actuators produce the actuation strain that physically causes induced strains to be produced. The actuators are used as modal actuators [42], which actuate the modal coordinate of a particular mode of the panel. They are also used to excite and measure combinations of modes [44] when they are used as sensors.

The piezoelectric layers are also assumed to be segmented so that only the desired portions of the piezoelectric layers are activated. This arrangement provides the opportunity to consider the piezoelectric materials as patches at the activated areas only. The mechanical/electrical behavior of the flexible panel are monitored or modified with these piezoelectric layers or patches acting as actuators and sensors. The piezoelectric patches are taken to be rectangular in shape; therefore, the piezoelectric layer is divided into N_c^x by N_c^y elements. E_3^t and E_3^b are the electric fields on the top and bottom piezoelectric layers, respectively. The overall thickness of the panel is h, the length of the panel in the air flow direction is a, and the span is b. The thickness of each piezoelectric patch or layer is h_p, and the thickness of the host layer is h_s. The geometrical properties of the panel are shown in Fig. (3.1).

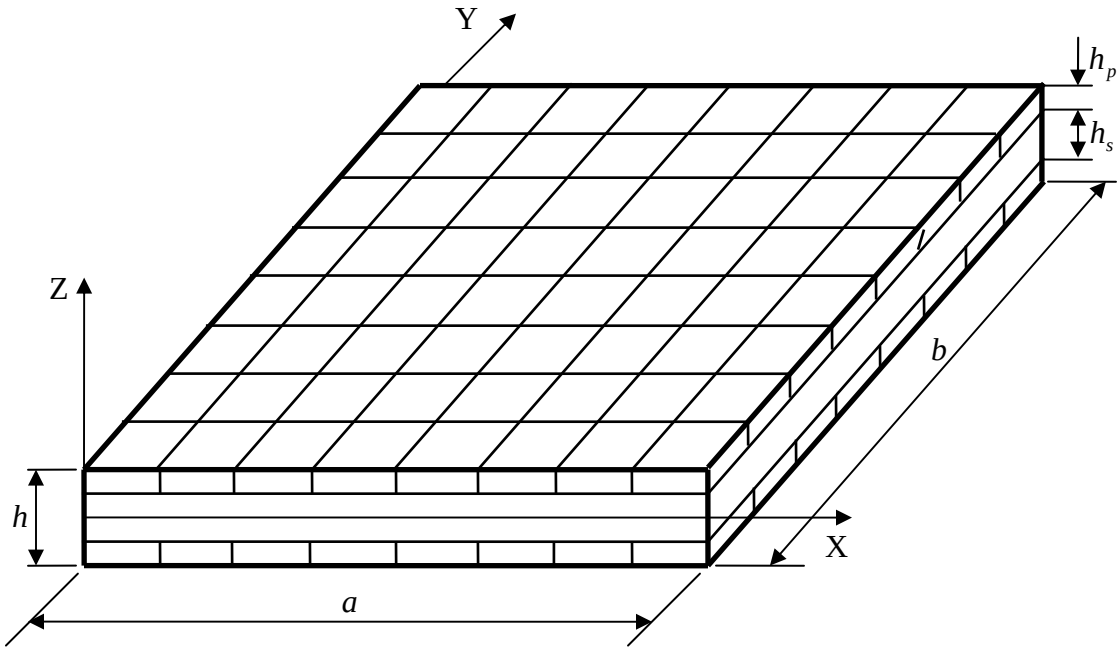

Fig. 3.1 Geometrical properties of a panel with bonded piezoceramic patches.

The inplane force induced by the piezoelectric layers, or patches per unit length or simply piezoelectric force per unit length is represented as

$$\left\{N^p\right\} = \int_{-\frac{h}{2}}^{\frac{h}{2}} \left[\overline{Q}\right]_k \left\{\varepsilon^p\right\}_k dz - \int_{-\frac{h_s}{2}}^{\frac{h_s}{2}} \left[\overline{Q}\right]_k \left\{\varepsilon^p\right\}_k dz \tag{3.16}$$

$$N_{xx}^p = 2\frac{E_p}{1-\nu^2} h_p \left(d_{31} + \nu d_{32}\right) E_m$$

$$= 2\frac{E_p}{1-\nu} h_p d_{31} E_m \tag{3.17a}$$

$$N_{yy}^p = 2\frac{E_p}{1-\nu^2} h_p \left(\nu d_{31} + d_{32}\right) E_m$$

$$= 2\frac{E_p}{1-\nu} h_p d_{31} E_m \tag{3.17b}$$

and

$$N_{xy}^{p} = 0 \tag{3.17c}$$

Where E_3 is the effective electric field applied on the top and bottom layers which produces only in-plane force, and denoted by E_m given as

$$E_m = \frac{1}{2}\left(E_3^t + E_3^b\right) \tag{3.18}$$

The induced bending moment actuation per unit length, or simply the piezoelectric bending moment per unit length is

$$\left\{M^p\right\} = \int_{-\frac{h}{2}}^{\frac{h}{2}} \left[\overline{Q}\right]_k \left\{\varepsilon^p\right\}_k z dz - \int_{-\frac{h_s}{2}}^{\frac{h_s}{2}} \left[\overline{Q}\right]_k \left\{\varepsilon^p\right\}_k z dz \tag{3.19}$$

where E_3 is the effective electric field applied on the top and bottom layers, which in this case is referred to as E_{bij} producing only bending moment, and it is given as

$$E_{bij} = \frac{1}{2}\left(E_{3ij}^t - E_{3ij}^b\right) \tag{3.20}$$

and defining

$$R_{31} = \frac{E_p}{1-\upsilon} d_{31} h_p \left(h_p + h_s\right)$$
$$R_{32} = \frac{E_p}{1-\upsilon} d_{31} h_p \left(h_p + h_s\right) \tag{3.21a,b}$$

The piezoelectric induced bending moment actuation due to discontinuously attached or embedded piezoelectric patches [54] can be written as

$$M_x^P = \sum_{i=1}^{N_c^x}\sum_{j=1}^{N_c^y} R_{31} E_{bij} \left[H\left(x - x_{i-1}\right) - H\left(x - x_i\right)\right]\left[H\left(y - y_{j-1}\right) - H\left(y - y_j\right)\right]$$

$$M_y^P = \sum_{i=1}^{N_c^x}\sum_{j=1}^{N_c^y} R_{32} E_{bij} \left[H\left(x - x_{i-1}\right) - H\left(x - x_i\right)\right]\left[H\left(y - y_{j-1}\right) - H\left(y - y_j\right)\right] \tag{3.22a,b}$$

where the Heaviside function H is given by

$$H(x-a)=\begin{cases}1 & x \geq a \\ 0 & x < a\end{cases} \tag{3.23}$$

$$\delta(x-a)=\frac{\partial}{\partial x}[H(x-a)]$$

$$\int_{-\infty}^{\infty}\delta^{n}(x-a)g(x)dx = g^{(n)}(a)(-1)^{n}$$

3.8 Nonlinear Equations of Motion

The governing differential equations for an isotropic plate with finite length and piezoelectric ceramic actuators bonded as patches or layers on a host plate subject to large deflection due to flow velocity over its surface and combined equivalent inplane loads, combined equivalent bending moments, aerodynamic load, and static pressure differential are derived in [67, 24]. The inclusion of piezoelectric terms can also be reviewed in [54]. The von Kármán's large deflection plate equations are represented as

$$D\nabla^{4}w=\frac{\partial^{2}\Phi}{\partial y^{2}}\frac{\partial^{2}w}{\partial x^{2}}+\frac{\partial^{2}\Phi}{\partial x^{2}}\frac{\partial^{2}w}{\partial y^{2}}-2\frac{\partial^{2}\Phi}{\partial x\partial y}\frac{\partial^{2}w}{\partial x\partial y}-\Delta^{s}p-m_{o}\frac{\partial^{2}w}{\partial t^{2}}-\frac{\partial^{2}M_{x}^{c}}{\partial x^{2}}-\frac{\partial^{2}M_{y}^{c}}{\partial y^{2}}+N_{x}^{c}\frac{\partial^{2}w}{\partial x^{2}}+N_{y}^{c}\frac{\partial^{2}w}{\partial y^{2}}-\Delta^{a}p \tag{3.24}$$

$$\frac{1}{Eh}\nabla^{4}\Phi=\left(\frac{\partial^{2}w}{\partial x\partial y}\right)^{2}-\left(\frac{\partial^{2}w}{\partial x^{2}}\right)\left(\frac{\partial^{2}w}{\partial y^{2}}\right) \tag{3.25}$$

The plate deflection is w, $m_{o}=\rho_{s}h_{s}+2\rho_{p}h_{p}$, Φ is the Airy stress potential function, N_{x}^{c}, N_{y}^{c} are combined equivalent inplane loads, and M_{x}^{c}, M_{y}^{c} are combined equivalent bending moments.

The aerodynamic pressure loading is assumed to be

$$\Delta^s p = p - p_\infty = \frac{2q}{\beta}\left[\frac{\partial w}{\partial x} + \left(\frac{M^2-2}{M^2-1}\right)\frac{1}{U}\frac{\partial w}{\partial t}\right] \tag{3.26}$$

Membrane inplane loads are given by

$$N_x^m = \alpha\frac{Eh}{2a}\int_0^a\left(\frac{\partial w}{\partial x}\right)^2 dx\,,\ N_y^m = \alpha\frac{Eh}{2a}\int_0^b\left(\frac{\partial w}{\partial y}\right)^2 dy$$

Induced piezoelectric inplane loads are given by

$$N_x^p = 2\frac{E_p}{1-\nu}h_p d_{31}E_m,\quad N_y^p = 2\frac{E_p}{1-\nu}h_p d_{31}E_m$$

Induced piezoelectric bending moments are given by

$$M_x^P = \sum_{i=1}^{N_c^x}\sum_{j=1}^{N_c^y} R_{31}E_{bij}\left[H(x-x_{i-1}) - H(x-x_i)\right]\left[H(y-y_{j-1}) - H(y-y_j)\right]$$

$$M_y^P = \sum_{i=1}^{N_c^x}\sum_{j=1}^{N_c^y} R_{32}E_{bij}\left[H(x-x_{i-1}) - H(x-x_i)\right]\left[H(y-y_{j-1}) - H(y-y_j)\right]$$

The inplane stress resultants are

$$N_x = \frac{\partial^2\Phi}{\partial y^2}$$

$$N_y = \frac{\partial^2\Phi}{\partial x^2}$$

$$N_{xy} = -\frac{\partial^2\Phi}{\partial x\partial y} \tag{3.27}$$

The inplane equations of equilibrium:

$$\frac{\partial N_x}{\partial x} + \frac{\partial N_{xy}}{\partial y} = 0$$

$$\frac{\partial N_y}{\partial y} + \frac{\partial N_{xy}}{\partial x} = 0 \tag{3.28}$$

are satisfied by Φ, the Airy stress potential function.

The boundary conditions for a plate that is simply-supported on the four edges are

$$u(0,y) = u(a,y) = w(0,y) = w(a,y) = \frac{\partial^2 w(0,y)}{\partial x^2} = \frac{\partial^2 w(a,y)}{\partial x^2} = 0 \tag{3.29}$$

$$v(x,0) = v(x,b) = w(x,0) = w(x,b) = \frac{\partial^2 w(x,0)}{\partial y^2} = \frac{\partial^2 w(x,b)}{\partial y^2} = 0 \tag{3.30}$$

The solution to the nonlinear equation given in Eq. (3.24), which is the displacement, can be represented as combination of linearly independent mode shapes. The assumed solutions must satisfy the given boundary conditions given in Eq. (3.29) and Eq. (3.30). Therefore, for a rectangular plate, simply-supported on all edges, one can assume that the transverse deflection can be written as

$$w = \sum_n \sum_m A_{nm} \sin\left(\frac{n\pi x}{a}\right) \sin\left(\frac{m\pi y}{b}\right) \tag{3.31}$$

with the longitudinal axis of the plate in the flow direction. One can simply retain only the first spanwise mode for panel flutter limit cycle analyses, hence $m = 1$, and the transverse deflection can be simplified as

$$w = \sum_n A_n \sin\left(\frac{n\pi x}{a}\right) \sin\left(\frac{\pi y}{b}\right) \tag{3.32}$$

Therefore, substituting Eq. (3.32) into Eq. (3.24) above [24], one obtains the nonlinear differential equations in time, and Lai et al. [54] obtained the additional term for piezoelectric bending moment:

$$\frac{d^2a_n}{d\tau^2}+\sqrt{\lambda c_a}\frac{da_n}{d\tau}+\pi^4\left[n^2+\left(\frac{a}{b}\right)^2\right]^2 a_n+\pi^2\left[R_x n^2+R_y\left(\frac{a}{b}\right)^2\right]a_n+\lambda\sum_r\frac{2nr}{n^2-r^2}\left[1-(-1)^{n+r}\right]a_r$$

$$+\pi^4\frac{Eh^3}{4D}\left\{\frac{a_n}{2}\left[n^2C_1+\left(\frac{a}{b}\right)^2C_2\right]+\left(\frac{a}{b}\right)^4\left(C_3+C_4+\frac{C_5}{4}-\frac{C_6}{2}\right)\right\}$$

$$=\frac{4a^3}{Dhb}R_{31}\left[\frac{nb}{a}+\frac{a}{nb}\left(\frac{a}{b}\right)^2\right]\sum_{i=1}^{N_c^x}\sum_{j=1}^{N_c^y}E_{bij}\cos\left(\frac{n\pi x}{a}\right)\Bigg|_{x_{i-1}}^{x_i}\cos\left(\frac{\pi y}{b}\right)\Bigg|_{y_{j-1}}^{y_j} \tag{3.33}$$

using the below non-dimensional quantities

$$a_n=\frac{A_n}{h},\ \tau=t\left(\frac{D}{m_0a^4}\right)^{\frac{1}{2}},\ R_x=-\frac{a^2}{D}N_x^c,\ R_y=-\frac{a^2}{D}N_y^c$$

$$\lambda=\frac{2qa^3}{M_\infty D},\ \lambda=\frac{2qa^3}{\beta D}$$

$$\mu=\frac{\rho_\infty a}{m_0},\ c_a=\frac{\mu}{M_\infty},\ c_a=\left(\frac{M_\infty^2-2}{M_\infty^2-1}\right)^2\left(\frac{\mu}{\beta}\right)$$

3.9 Nonlinear Modal Equations

Approximate deflections of the given system can be obtained using a linear combination of two modes. Hence, the modal nonlinear equations lead to a set of two coupled nonlinear differential equations, and they are given as

For $n=1$:

$$\frac{d^2a_1}{d\tau^2}+\sqrt{\lambda c_a}\frac{da_1}{d\tau}+\pi^4\left[n^2+\left(\frac{a}{b}\right)^2\right]^2 a_1+\pi^2\left[R_x n^2+R_y\left(\frac{a}{b}\right)^2\right]a_1-\lambda\frac{8}{3}a_2$$

$$+\pi^4\frac{Eh^3}{4D}\left\{\frac{a_1}{2}\left[n^2C_1+\left(\frac{a}{b}\right)^2C_2\right]+\left(\frac{a}{b}\right)^4\left(C_3+C_4+\frac{C_5}{4}-\frac{C_6}{2}\right)\right\}$$

$$= \frac{4a^3}{Dhb} R_{31} \left[\frac{nb}{a} + \frac{a}{nb} \left(\frac{a}{b} \right)^2 \right] \sum_{i=1}^{N_c^x} \sum_{j=1}^{N_c^y} E_{bij} \cos\left(\frac{n\pi x}{a} \right) \Bigg|_{x_{i-1}}^{x_i} \cos\left(\frac{\pi y}{b} \right) \Bigg|_{y_{j-1}}^{y_j} \tag{3.34a}$$

For $n = 2$:

$$\frac{d^2 a_2}{d\tau^2} + \sqrt{\lambda c_a} \frac{da_2}{d\tau} + \pi^4 \left[n^2 + \left(\frac{a}{b} \right)^2 \right]^2 a_2 + \pi^2 \left[R_x n^2 + R_y \left(\frac{a}{b} \right)^2 \right] a_2 + \lambda \frac{8}{3} a_1$$

$$+ \pi^4 \frac{Eh^3}{4D} \left\{ \frac{a_2}{2} \left[n^2 C_1 + \left(\frac{a}{b} \right)^2 C_2 \right] + \left(\frac{a}{b} \right)^4 \left(C_3 + C_4 + \frac{C_5}{4} - \frac{C_6}{2} \right) \right\}$$

$$= \frac{4a^3}{Dhb} R_{31} \left[\frac{nb}{a} + \frac{a}{nb} \left(\frac{a}{b} \right)^2 \right] \sum_{i=1}^{N_c^x} \sum_{j=1}^{N_c^y} E_{bij} \cos\left(\frac{n\pi x}{a} \right) \Bigg|_{x_{i-1}}^{x_i} \cos\left(\frac{\pi y}{b} \right) \Bigg|_{y_{j-1}}^{y_j} \tag{3.34b}$$

C_1, C_2, C_3, C_4, C_5 and C_6 are nonlinear terms of the modal amplitudes, and they are defined in the appendix.

The above equations can be rewritten by defining their coefficients with the quantities defined in the appendix, and these equations become

$$\ddot{a}_1 + c_d \dot{a}_1 - c_{fv} a_2 + c_{k3} a_1 + c_{330} a_1^3 + c_{312} a_1 a_2^2 = b_3 u$$

$$\ddot{a}_2 + c_d \dot{a}_2 + c_{fv} a_1 + c_{k4} a_2 + c_{403} a_2^3 + c_{421} a_1^2 a_2 = b_4 u \tag{3.35}$$

with a_1 and a_2 as the amplitudes of the first mode and second mode, respectively, and the coupling is caused by both the nonlinear terms and the flow velocity over the flat panel. The coefficients, c_d, c_{fv}, c_{k3}, c_{k4}, c_{312}, c_{330}, c_{403}, and c_{421}, of the two coupled nonlinear ordinary differential equations in Eq. (3.35) are non-negative quantities, which are easily obtained by expansion and collection of the coefficients of the modal amplitudes a_1 and

a_2 and their derivatives. One writes the equations of motion in Eq. (3.35) as a set of first-order differential equations using state space format. State variables are defined as

$$\{x_1, x_2, x_3, x_4\}^T = \{a_1, a_2, \dot{a}_1, \dot{a}_2\}^T$$

and the system with Single Input can be written as:

$$\dot{x} = f(x) + g(x)u \tag{3.36}$$

$$y = h(x) \tag{3.37}$$

where,

$$f(x) = \begin{Bmatrix} x_3 \\ x_4 \\ c_{fv}x_2 - c_{k3}x_1 - c_d x_3 - c_{330}x_1^3 - c_{312}x_1 x_2^2 \\ -c_{fv}x_1 - c_{k4}x_2 - c_d x_4 - c_{403}x_2^3 - c_{421}x_1^2 x_2 \end{Bmatrix} \tag{3.36.a}$$

$$g(x) = \begin{Bmatrix} 0 \\ 0 \\ b_3 \\ b_4 \end{Bmatrix} \tag{3.36.b}$$

and $x \in R^n$ is the state vector, $u \in R^m$ is the control vector, and $f : R^n \to R^n$ is a sufficiently smooth nonlinear function of its argument. $g : R^n \to R^n$, is a sufficiently smooth nonlinear function of its argument.

4. FEEDBACK LINEARIZATION

The mathematical modeling of most physical systems results in nonlinear systems, and in order to achieve the desired dynamic behavior for such systems, feedback control systems are often designed which make the closed-loop systems achieve the specified objectives. There are numerous ways to design a feedback control system. There are both linear and nonlinear feedback control systems. The former are usually based on an approximate linearized model of an actual nonlinear system about the equilibrium point, while the later are based on the actual nonlinear system. There are various types of nonlinear control techniques, and these include a technique called feedback linearization.

Feedback linearization is achieved by exact state transformations and feedback, rather than by linear approximations to the system dynamics, and this implies that the original system models are transformed into equivalent linear models of a simpler form. Feedback linearization problems have attracted considerable attention, and have been used successfully in practical control problems, such as control of helicopters, high performance aircraft, industrial robots, and biomedical devices.

Panel flutter with its associated limit cycle motions, if not suppressed, can lead to failure of the panel. Flutter suppression of a panel with distributed and embedded or bonded active materials can be achieved using feedback control with distributed active materials acting as sensors and actuators, or self-sensing actuators.

The sensors can be made to sense the outputs (motions) of the panel, and the sensed signals are modified by the feedback controllers and then used to actuate the panel through the actuators. This active system is used to stabilize the motion of the panel so that the states have a locally asymptocally stable origin, which is the main control objective.

Design of linear controllers requires that an equilibrium point be selected, usually the system origin, and corresponding to the state of a panel without deflection. The formulated nonlinear system is linearized about this equilibrium point with the assumption that there are only very small displacements of the states from the origin, but in panel fluttering these displacements can be large, therefore, the assumption of small displacements about the origin is invalid. The design of linear feedback controllers only extends the flutter free region of the panel; it does not effectively suppress the fluttering, since fluttering involves large displacements from the origin.

With feedback linearization, the nonlinear panel flutter problem is transformed using output feedback into an equivalent controllable linear system that is in simple Brunovsky canonical form. This involves the formulation of nonlinear feedback control laws, which cancel the nonlinear dynamics. The pole placement technique is then employed to make the states of the feedback linearized model locally asymptotically stable to the origin.

4.1 Mathematical Background

In this section, the mathematical tools required for linearization by feedback control are developed. The nonlinear control system is first transformed into the Brunovsky form by a change of coordinates and state feedback, and then linear controllers are designed to control the linearized system. A thorough review of feedback linearization can be found in the literature [68-69].

A single-input single-output (SISO) closed-loop system is given in Eq. (4.1) below:

$$\dot{x} = f(x) + g(x)u \tag{4.1a}$$

$$y = h(x) \tag{4.1b}$$

where $x \in R^n$ is a vector of states, $u \in R^p$ is the input vector, $y \in R^m$, f and g are smooth vector fields on R^n and h a smooth (i.e., an infinitely differentiable) nonlinear function.

If the input feedback u and coordinate transformations of the states $\Phi(x)$ are applied, such that,

$$u = \alpha(x) + \beta(x)v \tag{4.2}$$

$$z = \Phi(x) \tag{4.3}$$

where v is the external reference input, and the coordinate transformation $\Phi(x)$ has the following properties

(i) $\Phi(x)$ is invertible, $\forall x \in R^n$

(ii) $\Phi(x)$ and $\Phi^{-1}(z)$ are both smooth mappings

then, $\Phi(x)$ is the "normal form" of special interest, which provides suitable change of coordinates in the state space. The nonlinear closed-loop system in Eq. (4.1) is transformed to the new coordinates to become a linear closed-loop system given in Eq. (4.4).

$$\dot{z} = Az + Bv \tag{4.4}$$

4.1.1 Lie derivatives

Let $h : R^n \to R$ be a smooth scalar function, and $f : R^n \to R^n$ be a smooth vector field on R^n, then the Lie derivative $L_f h(x)$ is the directional derivative of a function $h(x)$ along the direction of the vector $f(x)$.

$$L_f h(x) : R^n \mapsto R,$$

$$L_f h(x) = \frac{\partial h(x)}{\partial x} \cdot f(x) \tag{4.5}$$

Lie derivatives may be generated recursively, and they are defined as

$$L_f^0 h = h \tag{4.6a}$$

$$L_f^i h = L_f\left(L_f^{i-1} h\right) = \frac{\partial\left(L_f^{i-1} h\right)}{\partial x} \cdot f, \; i = 1,2,\ldots,n \tag{4.6b}$$

Similarly, if $g : R^n \to R^n$ is a smooth vector field, then

$$L_g h(x) : R^n \mapsto R$$

$$L_g h(x) = \frac{\partial h(x)}{\partial x} \cdot g(x) \tag{4.7}$$

also, the scalar function $L_g L_f h(x)$ is defined as

$$L_g L_f h(x) = \frac{\partial\left(L_f h(x)\right)}{\partial x} g(x) \tag{4.8}$$

4.1.2 Lie Bracket

Let f and g be two vector fields on R^n. The Lie bracket of f and g written as $[f,g]$ is a third vector defined as

$$[f,g]=\frac{\partial g(x)}{\partial x}f(x)-\frac{\partial f(x)}{\partial x}g(x) \tag{4.9a}$$

$$[f,g]=L_g f - L_f g = ad_f g \tag{4.9b}$$

Repeated Lie brackets can be defined recursively by,

$$ad_f^0 g = g \tag{4.10a}$$

$$ad_f^0 g = [f, ad_f^{i-1} g], \qquad i = 1,2,\ldots,n \tag{4.10b}$$

4.1.3 Frobenius Theorem

A nonsingular distribution $\Delta = span\{f_1, f_2,\ldots, f_m\}$ is completely integrable if, and only if, it is involutive. The distribution Δ is involutive if the Lie bracket $[f_i, f_j]$ of any pair of vector fields f_i and f_j belongs to the distribution Δ, that is,

$$f_i \in \Delta,\ f_j \in \Delta \Rightarrow [f_i, f_j] \in \Delta \tag{4.11}$$

where $f_i,\ldots, f_m$ are smooth vector fields locally spanning Δ.

4.1.4 Diffeomorphisms and State Trannsformations

A function $\Phi : R^n \rightarrow R^n$, defined in a region Ω, is called a diffeomorphism if it is smooth, and if its inverse Φ^{-1} exists and is smooth. If the region Ω is the whole space R^n, then $\Phi(x)$ is called a global diffeomorphism, but if the transformations are

defined only in a finite neighborhood of a given point, then it is a local diffeomorphism about the given point.

4.1.5 Controllability

A system is said to be controllable if and only if it is possible, by means of the input, to transfer the system from any initial state $x(t_0) = x_0$, to any other state $x(t_f) = x_f$ in a finite time $t_f - t_0 \geq 0$. The controllability matrix for a nonlinear system in Eq. (4.12) is given by

$$C = \left[g_1 \quad ,\ldots, \quad g_m, \quad ad_f g_1 \quad ,\ldots, \quad ad_f g_m, \quad ad_f^{r-1} g_1 \quad ,\ldots, \quad ad_f^{r-1} g_m \right] \qquad (4.12)$$

with relative degree, $r \leq n$

4.2 Single-Input Single Output (SISO) System

Consider a single-input single output (SISO) nonlinear system of the form given in Eq. (4.1).

4.2.1 Relative degree

The system given by Eq. (4.1) is said to have a relative degree r at a particular point x_0 if

$L_g L_f^{i-1} h(x) = 0$, for all x in a neighborhood of x_0 $\qquad i = 1,2,\ldots,r-1$

$L_g L_f^{r-1} h(x) \neq 0$

Intuitively, relative degree is the number of times one has to differentiate the output function, $h(x)$ to obtain an expression where the input u appears explicitly.

4.2.2 Exact linearization

Full feedback linearization or exact linearization is carried out when the relative degree of the nonlinear system is the same as the dimension of the system, that is $r = n$. Consider a SISO (Single-Input, Single-Output) nonlinear system

$$\dot{x} = f(x) + g(x)u$$

$$y = h(x)$$

repeatedly differentiating the output

$$\dot{y} = \frac{\partial h}{\partial x}\dot{x}$$

$$= \frac{\partial h}{\partial x}\left[f(x) + g(x)u\right]$$

$$= L_f h(x) + L_g h(x)u \tag{4.14}$$

where $L_f h(x) \equiv \frac{\partial h}{\partial x} f(x)$, $\quad L_g h(x) \equiv \frac{\partial h}{\partial x} g(x)$

by repeated differentiations of the output y, r times, we obtain

$$L_g L_f^{i-1} h(x) = 0, \quad i = 1,2,\ldots,r-1 \tag{4.15a}$$

$$L_g L_f^{r-1} h(x) \neq 0 \tag{4.15b}$$

$$L_g L_f^{i} h(x) = L_g\left[L_f^{i} h(x)\right], \tag{4.15c}$$

$$L_f^{i} h(x) = L_f\left[L_f^{i-1} h(x)\right], \quad i = 1,2,\ldots,r-1, \tag{4.15d}$$

and $L_f^0 h(x) \equiv h(x)$

$$y^{(r)} = L_f^r h(x) + L_g L_f^{r-1} h(x)u \tag{4.16}$$

for reference trajectory

$$y^{(r)} = v \tag{4.17}$$

where the new input v is chosen to cancel the nonlinear dynamics in Eq. (4.16), that is,

$$u = \frac{v - L_f^r h(x)}{L_g L_f^{r-1} h(x)}, \tag{4.18}$$

4.2.2.1 Nonlinear coordinate transformation:

The nonlinear system is transformed to the normal form by r functions $h(x)$, $L_f h(x), \ldots, L_f^{n-1} h(x)$ when the relative degree is same as the system dimension, that is, $r = n$, and these form a new set of coordinate functions around the point x_0.

$$z = \Phi(x) = \begin{bmatrix} h \\ L_f h \\ L_f^2 h \\ \vdots \\ L_f^{n-1} h \end{bmatrix}, \tag{4.19}$$

$x = \Phi^{-1}(z)$ exists and is unique $\forall x \in R^n$, so that

$$\dot{z}_1 = z_2$$

$$\dot{z}_2 = z_3$$

$$\vdots$$

$$\dot{z}_n = L_f^n h(x) + L_g L_f^{n-1} h(x) u(t) \text{ or } \dot{z}_r = b(z) + a(z)u \tag{4.20}$$

Output

$$y = z_1 \tag{4.21}$$

For reference trajectory

$$\dot{z}_r = v \tag{4.22}$$

where

$$u = \frac{1}{a(\Phi(z))}\left(-b(\Phi(z)) + v\right) \tag{4.23a}$$

or

$$u = \frac{1}{L_g L_f^{r-1} h(x)}\left(-L_f^r h(x) + v\right) \tag{4.23b}$$

4.2.3 Partial linearization

Nonlinear system with relative degree less than the dimension of the system ($r < n$) cannot be fully feedback linearized, but can only be partially linearized. In this case, it can be transformed into the "normal form" of the feedback linearization.

4.2.3.1 Nonlinear coordinate transformation:

In the case where the relative degree is less than the system dimension, that is, $r < n$, r functions $h(x),\ L_f h(x), \ldots, L_f^{r-1} h(x)$ provide a partial set of new coordinate functions around the point x_0. It is possible to find $n - r$ more functions $\phi_{r+1}(x), \ldots, \phi_n(x)$ so that

$L_g \phi_i(x) = 0 \qquad \forall r+1 \le i \le n$ and $\forall x$ around x_0

The nonlinear system is transformed into the normal form by these functions.

$$\Phi : x \mapsto \begin{bmatrix} h \\ L_f h \\ \vdots \\ L_f^{r-1} h \\ \eta \end{bmatrix}, \tag{4.24}$$

$x = \Phi^{-1}(\xi, \eta)$ exists and is unique $\forall x \in R^n$

Therefore, the new variables are $h, L_f h, \ldots, L_f^{r-1}$ in ξ coordinates, and $\phi_{r+1}(x), \ldots, \phi_n(x)$ in η coordinates. The nonlinear system is transformed to the new (ξ, η) coordinates, that is,

$$\dot{\xi}_1 = \xi_2$$

$$\dot{\xi}_2 = \xi_3$$

$$\vdots$$

$$\dot{\xi}_r = b(\xi, \eta) + a(\xi, \eta) u(t)$$

$$\dot{\eta} = q(\xi, \eta) \tag{4.25}$$

Output

$$y = \xi_1 \tag{4.26}$$

for reference trajectory

$$\dot{\xi}_r = v \tag{4.27}$$

hence, choosing the new input as

$$v = b(\xi, \eta) + a(\xi, \eta) u(t) \tag{4.28}$$

where, $b(\xi, \eta) = L_f^r h(\Phi^{-1}(\xi, \eta))$, (4.29a)

$$a(\xi, \eta) = L_g L_f^{r-1} h(\Phi^{-1}(\xi, \eta)) \tag{4.29b}$$

The original input can be written as

$$u = \frac{1}{a(\Phi(\xi,\eta))}\left(-b(\Phi(\xi,\eta)) + v\right) \tag{4.30a}$$

or,

$$u = \frac{1}{L_g L_f^{r-1} h(x)}\left(-L_f^r h(x) + v\right) \tag{4.30b}$$

The system in Eq. (4.25) is partially linear. The system is decomposed into a linear subsystem with r^{th}-order dynamics and a possibly nonlinear subsystem with $(n-r)^{th}$-order dynamics, which has been rendered unobservable, and this part of the dynamics describes the internal behavior of the system, and it is referred to as the internal dynamics. It is given by

$$\dot{\eta} = q(\xi,\eta)$$

It is necessary to check the stability of the internal dynamics so as to determine if it is stable, otherwise, the feedback linearized system is useless. Therefore, the internal behavior of the system is studied when the input and the initial conditions are chosen so as to constrain the output to remain identically zero, and this is called the zero dynamics, and it is given by

$$\dot{\eta} = q(0,\eta)$$

4.3 Multi-Input Multi-Output (MIMO) System

Consider a MIMO (Multi-Input, Multi-Output) nonlinear system of the form given in Eq. (4.31). In this analysis, it is assumed that the system has the same number, m, of input and output channels.

$$\dot{x} = f(x) + \sum_{i=1}^{m} g_i(x) u_i \tag{4.31a}$$

$$y_1 = h_1(x)$$

$$\vdots$$

$$y_m = h_m(x) \tag{4.31b}$$

The outputs can be repeatedly differentiated until one of the outputs appears explicitly. If r_i is assumed to be the smallest integer, then,

$$y_i^{r_i} = L_f^{r_i} h_i + \sum_{j=1}^{m} \left(L_{g_j} L_f^{r_i - 1} h_i u_j \right) \tag{4.32}$$

with $L_{g_j} L_f^{r_i - 1} h_i u_j \neq 0$, for at least one j

If at least one of the inputs appears at r_j differentiation in $y_j^{r_j}$, such that, $L_{g_i} L_f^{r_j - 1} \neq 0$, then one can define a matrix $E(x) \in R^{m \times m}$, such that

$$E(x) = \begin{bmatrix} L_{g_1} L_f^{r_1 - 1} h_1(x) & \cdots & L_{g_m} L_f^{r_1 - 1} h_1(x) \\ \vdots & \ddots & \vdots \\ L_{g_1} L_f^{r_m - 1} h_m(x) & \cdots & L_{gm} L_f^{r_m - 1} h_m(x) \end{bmatrix} \tag{4.33}$$

A system is said to have vector relative degree, $\{r_1, \ldots, r_m\}$ at x_0, if

$$L_{g_i} L_f^k h_i(x) \equiv 0, \quad 0 \leq k \leq r_i - 2$$

for, $i = 1, \ldots, m$, and the matrix $E(x_0)$ is nonsingular [sastry].

$r_1 + \ldots + r_m \leq n$, and total scalar relative degrees is given by $r = r_1 + \ldots + r_m$

4.3.1 Nonlinear coordinate transformation:

The normal form for MIMO nonlinear system is obtained based on the functions $h_i(x),\ L_f h_i(x), \ldots, L_f^{r_i - 1} h_i(x)$ generated by the Lie derivatives in Eq. (4.32).

$$\phi_1^i = h_i$$

$$\phi_2^i = L_f h_i$$

$$\vdots$$

$$\phi_{r_i}^i = L_f^{r_i - 1} h_i, \qquad \text{for } 1 \le i \le m$$

$$\Phi(x) = col\left[\phi_1^1(x) \quad ,\ldots, \quad \phi_{r_i}^1(x), \quad ,\ldots, \quad \phi_m^1(x) \quad ,\ldots, \quad \phi_{r_m}^1(x), \quad \phi_{r+1}^1(x) \quad ,\ldots, \quad \phi_m^1(x)\right]$$

from the differentiations in Eq. (4.32), one can write;

$$\begin{Bmatrix} y_1^{r_1} \\ \vdots \\ y_m^{r_m} \end{Bmatrix} = \begin{Bmatrix} L_f^{r_1} h_1 \\ \vdots \\ L_f^{r_1} h_m \end{Bmatrix} + E(x) \begin{Bmatrix} u_1 \\ \vdots \\ u_m \end{Bmatrix} \tag{4.34a}$$

hence the state feedback control laws are formulated so that the nonlinear dynamics can be cancelled, and they are written as;

$$\begin{Bmatrix} u_1 \\ \vdots \\ u_2 \end{Bmatrix} = E^{-1}(x) \begin{Bmatrix} L_f^{r_1} h_1 \\ \vdots \\ L_f^{r_1} h_1 \end{Bmatrix} + E^{-1}(x) \begin{Bmatrix} y_1^{r_1} \\ \vdots \\ y_m^{r_m} \end{Bmatrix}$$

or

$$u = E^{-1}(x) \begin{Bmatrix} L_f^{r_1} h_1 \\ \vdots \\ L_f^{r_1} h_1 \end{Bmatrix} + E^{-1}(x) v \tag{4.34b}$$

for the reference trajectories

$$\begin{Bmatrix} y_1^{r_1} \\ \vdots \\ y_m^{r_m} \end{Bmatrix} = \begin{Bmatrix} v_1 \\ \vdots \\ v_m \end{Bmatrix} \tag{4.34c}$$

and these yield the linear closed loop system represented as

$$\dot{\xi}_1^i = \xi_2^i$$

$$\vdots$$

$$\dot{\xi}^i_{r_i-1} = \xi^i_{r_i}$$

$$\dot{\xi}^i_{r_i} = b_i(\xi,\eta) + \sum_j^m a^i_j(\xi,\eta)u_j(t) \tag{4.35a}$$

$$y_i = \xi^i_1 \tag{4.35b}$$

4.4 Application to Panel Flutter Suppression

The technique of linearizing a nonlinear system by feedback control presented in Section 4.1 is applied to the resulting nonlinear system from the mathematical modeling of a flat panel with embedded or bonded distributed piezoelectric patches subjected to both aerodynamic loads and externally applied inplane forces carried out in Chapter 3. The dynamic analysis reveals that vibrations with large amplitudes exist, and nonlinearities in the system give rise to limit cycle motions. The amplitudes of the vibrational modes are sensed by piezoelectric sensors, and these are represented as the outputs. The inputs are the actuation of the panel by the piezoelectric actuators. The output signals from the sensors are feedback through the linearizing controllers developed in this research to the actuators, and these are used to suppress the fluttering of the panel by placing the poles of the linearized system so they are stable.

4.4.1 Control with first mode as the ouput:

In this section, it is considered that the state-space representation of the panel fluttering dynamics has a single input signal fed to the actuators distributed over the surface of the panel and single output. Therefore, the analysis for single-input single-

output nonlinear system represented by Eq. (4.1) in Section 4.2 can be applied to the panel flutter nonlinear dynamics given by Eq. (3.36) and Eq. (3.37), and these presented as Eq. (4.36) below:

$$\dot{x} = f(x) + g(x)u \tag{4.36a}$$

$$y = h(x) \tag{4.36b}$$

where

$$f(x) = \begin{Bmatrix} x_3 \\ x_4 \\ c_{fv}x_2 - c_{k3}x_1 - c_d x_3 - c_{330}x_1^3 - c_{312}x_1 x_2^2 \\ -c_{fv}x_1 - c_{k4}x_2 - c_d x_4 - c_{403}x_2^3 - c_{421}x_1^2 x_2 \end{Bmatrix}$$

$$g(x) = \begin{Bmatrix} 0 \\ 0 \\ b_3 \\ b_4 \end{Bmatrix}$$

and the output function chosen is the amplitude of the first mode, and it is given as

$$y = h(x) = x_1$$

differentiating the chosen output

$$L_g L_f h = b_3 \neq 0 \;\Rightarrow \text{ relative degree, } r = 2$$

$$L_f^2 h = c_{fv}x_2 - c_{k3}x_1 - c_{312}x_1 x_2^2 - c_{330}x_1^3 - c_d x_3$$

Since the relative degree r is 2, while the system is a set of four first-order differential equations, then one can only carry out partial feedback linearization of the system with the chosen output, therefore, the x coordinates of the original domain becomes $x(\xi, \eta)$ in the transformed coordinates.

Using the computed Lie derivative, the normal form is given as:

$$\Phi = \begin{Bmatrix} \xi_1 \\ \xi_2 \\ \xi_3 \\ \xi_4 \end{Bmatrix} = \begin{Bmatrix} h \\ L_f h \\ \eta_1 \\ \eta_2 \end{Bmatrix} = \begin{Bmatrix} x_1 \\ x_3 \\ x_2 \\ b_4 x_3 - b_3 x_4 \end{Bmatrix} \tag{4.37}$$

where ξ_3 and ξ_4 are defined such that $L_g \eta_1 = 0$ and $L_g \eta_2 = 0$.

The Jacobian matrices of the transform and inverse transform are given below, and they are nonsingular and are well defined, since for any input, $b_3 \neq 0$.

$$\left| \frac{d\Phi}{dx} \right| = b_3$$

Therefore, this system with the chosen output has a transformation that is global diffeomorphism, and inversion of the coordination transformations can be carried out globally. The original states are obtained in terms of the linearizing coordinates as given in Eq. (4.18) below

$$x = \begin{Bmatrix} x_1 \\ x_2 \\ x_3 \\ x_4 \end{Bmatrix} = \begin{Bmatrix} \xi_1 \\ \eta_1 \\ \xi_2 \\ \dfrac{1}{b_3}\left(b_4 \xi_2 - \eta_2\right) \end{Bmatrix} \tag{4.38}$$

The system dynamics for panel flutter given in Eq. (4.36), is partially feedback linearized and it is represented in the new coordinates as

$$\begin{Bmatrix} \dot{\xi}_1 \\ \dot{\xi}_2 \\ \dot{\eta}_1 \\ \dot{\eta}_2 \end{Bmatrix} = \begin{Bmatrix} \xi_2 \\ c_{fv}\eta_1 - c_{k3}\xi_1 - c_{312}\eta_1^2\xi_1 - c_{330}\xi_1^3 - c_d\eta_2 \\ \frac{1}{b_3}(b_4\xi_2 - \eta_2) \\ -b_3\left(-c_{k4}\eta_1 - c_{403}\eta_1^3 - c_{fv}\xi_1 - c_{421}\xi_1^2\eta_1 - c_d\left(\frac{b_4\xi_2}{b_3} - \frac{\eta_2}{b_3}\right)\right) + b_4\left(c_{fv}\eta_1 - c_{k3}\xi_1 - c_{312}\xi_1\eta_1^2 - c_{330}\xi_1^3 - c_d\xi_2\right) \end{Bmatrix}$$

$$+ \begin{Bmatrix} 0 \\ b_3 \\ 0 \\ 0 \end{Bmatrix} u \tag{4.39}$$

and for reference trajectory:

$$v = \dot{\xi}_2$$

from eq. 4.19

$$\dot{\xi}_2 = L_f^2 h + L_g L_f h u$$

therefore, the control input u is designed to cancel the nonlinear dynamics, hence

$$u = \frac{v - L_f^2 h}{L_g L_f h},$$

$$u = \frac{1}{b_3}\left(v - \left(c_{fv}\eta_1 - c_{k3}\xi_1 - c_{312}\eta_1^2\xi_1 - c_{330}\xi_1^3 - c_d\eta_2\right)\right) \tag{4.40}$$

Output:

$$y = \xi_1 \tag{4.41}$$

Substituting Eq. (4.20) into Eq. (4.19), the resulting system is partially linearized with the linearized subsystem given as;

$$\begin{pmatrix} \dot{\xi}_1 \\ \dot{\xi}_2 \end{pmatrix} = \begin{pmatrix} 0 & 1 \\ 0 & 0 \end{pmatrix}\begin{pmatrix} \xi_1 \\ \xi_2 \end{pmatrix} + \begin{pmatrix} 0 \\ v \end{pmatrix} \tag{4.42}$$

They are made asymptotically stable by pole placements;

$v(\xi) = -K\xi$, or $v = -k_0\xi_1 - k_1\xi_2$

4.4.1.1 Internal dynamics

The internal dynamics are given by the subsystem below:

$$\dot{\eta}_1 = \frac{1}{b_3}\left(b_4\xi_2 - \eta_2\right)$$

$$\dot{\eta}_2 = -b_3\left(-c_{k4}\eta_1 - c_{403}\eta_1^3 - c_{fv}\xi_1 - c_{421}\xi_1^2\eta_1 - c_d\left(\frac{b_4\xi_2}{b_3} - \frac{\eta_2}{b_3}\right)\right) + b_4\left(c_{fv}\eta_1 - c_{k3}\xi_1 - c_{312}\xi_1\eta_1^2 - c_{330}\xi_1^3 - c_d\xi_2\right) \tag{4.43}$$

4.4.1.2 Zero dynamics

The zero dynamics are given below:

set $\eta = \{\eta_1, \eta_2, \xi_1, \xi_2\} = \{\eta_1, \eta_2, 0, 0\}$, hence,

$$\dot{\eta}_1 = -\frac{\eta_2}{b_3}$$

$$\dot{\eta}_2 = \left(b_4 c_{fv} + b_3 c_{k4}\right)\eta_1 - c_d\eta_2 - c_{403}\eta_1^3 \tag{4.44}$$

The feedback linearized subsystem presented in Eq. (4.42) is a second-order dynamic system, with the modal amplitude of the first mode and its derivative as the two new states in the transformed coordinates. The designed controllers are proportional to the two new states therefore the controlled subsystem simply becomes a damped mass spring oscillator in the new coordinates in terms of the first mode. The modal amplitude of the second mode and its derivatives constitute the zero dynamics presented in Eq. (4.44).

4.4.2 Control with second mode as the output:

In this case, the output from the system dynamics is taken as the amplitude of the second mode of the panel flutter sensed by the distributed sensors attached to the panel at appropriate locations, and a single input signal fed to the actuators distributed over the surface of the panel. Therefore, again, the analysis for single-input single-output nonlinear system in Section 4.2 can be applied also to the system presented in Eq. (4.36).

$$\dot{x} = f(x) + g(x)u$$

$$y = h(x)$$

$$f(x) = \begin{Bmatrix} x_3 \\ x_4 \\ c_{fv}x_2 - c_{k3}x_1 - c_d x_3 - c_{330}x_1^3 - c_{312}x_1 x_2^2 \\ -c_{fv}x_1 - c_{k4}x_2 - c_d x_4 - c_{403}x_2^3 - c_{421}x_1^2 x_2 \end{Bmatrix}$$

$$g(x) = \begin{Bmatrix} 0 \\ 0 \\ b_3 \\ b_4 \end{Bmatrix}$$

and the output is given as

$$y = h(x) = x_2 \tag{4.45}$$

differentiating the chosen output

$$L_g L_f h = b_4 \neq 0 \;\Rightarrow \text{ relative degree, } r = 2$$

$$L_f^2 h = -c_{fv}x_1 - c_{k4}x_2 - c_{421}x_1^2 x_2 - c_{403}x_2^3 - c_d x_4$$

The relative degree, r, is 2, while the system is a set of four first-order differential equation, therefore, one can only carry out partial feedback linearization of the system

with the chosen output, therefore, the x coordinate of the original domain becomes $x(\xi,\eta)$ in the transformed coordinates

Using the computed Lie derivatives, the normal form is given as:

$$\Phi = \begin{Bmatrix} \xi_1 \\ \xi_2 \\ \xi_3 \\ \xi_4 \end{Bmatrix} = \begin{Bmatrix} h \\ L_f h \\ \eta_1 \\ \eta_2 \end{Bmatrix} = \begin{Bmatrix} x_2 \\ x_4 \\ x_1 \\ b_4 x_3 - b_3 x_4 \end{Bmatrix} \tag{4.46}$$

where ξ_3 and ξ_4 are defined such that $L_g \eta_1 = 0$ and $L_g \eta_2 = 0$.

$$x = \begin{Bmatrix} x_1 \\ x_2 \\ x_3 \\ x_4 \end{Bmatrix} = \begin{Bmatrix} \eta_1 \\ \xi_1 \\ \frac{1}{b_4}\left(b_3 \xi_2 + \eta_2\right) \\ \xi_2 \end{Bmatrix} \tag{4.47}$$

The Jacobian matrices of the transform and inverse transform are given below, and they are nonsingular and are well defined, since for any input, $b_4 \neq 0$.

$$\left|\frac{d\Phi}{dx}\right| = -b_4$$

The partial feedback linearized system becomes:

$$\begin{Bmatrix} \dot{\xi}_1 \\ \dot{\xi}_2 \\ \dot{\eta}_1 \\ \dot{\eta}_2 \end{Bmatrix} = \begin{Bmatrix} \xi_2 \\ -c_{fv}\eta_1 - c_{k4}\xi_1 - c_{421}\eta_1^2\xi_1 - c_{403}\xi_1^3 - c_d\eta_2 \\ \frac{1}{b_4}\left(b_3\xi_2 + \eta_2\right) \\ -b_3\left(-c_{k4}\xi_1 - c_{403}\xi_1^3 - c_d\xi_2 - c_{fv}\eta_1 - c_{421}\xi_1\eta_1^2\right) + b_4\left(c_{fv}\xi_1 - c_{k3}\eta_1 - c_{312}\xi_1^2\eta_1 - c_{330}\eta_1^3 - c_d\left(\frac{b_3\xi_2}{b_4} + \frac{\eta_2}{b_4}\right)\right) \end{Bmatrix}$$

$$+\begin{Bmatrix} 0 \\ b_4 \\ 0 \\ 0 \end{Bmatrix} u \tag{4.48}$$

reference trajectory:

$$v = \dot{\xi}_2$$

from eq. 4.48

$$\dot{\xi}_2 = L_f^2 h + L_g L_f h u$$

therefore, input u is designed so that the nonlinear dynamics are cancelled.

$$u = \frac{v - L_f^2 h}{L_g L_f h},$$

$$u = \frac{1}{b_4}\left(v - \left(-c_{fv}\eta_1 - c_{k4}\xi_1 - c_{421}\eta_1^2\xi_1 - c_{403}\xi_1^3 - c_d\eta_2\right)\right)$$

Output:

$$y = \xi_1 \tag{4.49}$$

The linear subsystem of the feedback linearized system is given below:

$$\begin{pmatrix} \dot{\xi}_1 \\ \dot{\xi}_2 \end{pmatrix} = \begin{pmatrix} 0 & 1 \\ 0 & 0 \end{pmatrix}\begin{pmatrix} \xi_1 \\ \xi_2 \end{pmatrix} + \begin{pmatrix} 0 \\ v \end{pmatrix} \tag{4.50}$$

and by pole placements; $v(\xi) = -K\xi$, or $v = -k_0\xi_1 - k_1\xi_2$

The new control input v is chosen, so that Eq. (4.50) is linear and in canonic form, therefore, the linear control gains k_0 and k_1 are designed so that the subsystem is asymptotically stable.

4.4.2.1 Internal dynamics:

The internal dynamics are given by the subsystem below:

$$\dot{\eta}_1 = \frac{1}{b_4}\left(b_3\xi_2 + \eta_2\right)$$

$$\dot{\eta}_2 = -b_3\left(-c_{k4}\xi_1 - c_{403}\xi_1^3 - c_d\xi_2 - c_{fv}\eta_1 - c_{421}\xi_1\eta_1^2\right) + b_4\left(c_{fv}\xi_1 - c_{k3}\eta_1 - c_{312}\xi_1^2\eta_1 - c_{330}\eta_1^3 - c_d\left(\frac{b_3\xi_2}{b_4} + \frac{\eta_2}{b_4}\right)\right) \tag{4.51}$$

4.4.2.2 Zero dynamics

The zero dynamics are given below in Eq. (4.52), by setting:

$$\eta = \{\eta_1, \eta_2, \xi_1, \xi_2\} = \{\eta_1, \eta_2, 0, 0\},$$

hence,

$$\dot{\eta}_1 = \frac{\eta_2}{b_4}$$

$$\dot{\eta}_2 = \left(b_3 c_{fv} - b_4 c_{k3}\right)\eta_1 - c_d\eta_2 - b_4 c_{330}\eta_1^3 \tag{4.52}$$

As a reversal to the case in previous section, the feedback linearized subsystem presented in Eq. (4.50) is second-order, with the modal amplitude of the second mode and its derivative as the two new states in the transformed coordinates. The designed controllers are also chosen to be proportional to the two new states. The modal amplitude of the first mode and its derivatives constitute the zero dynamics presented in Eq. (4.52).

4.4.3 Control with both first and second modes as the outputs:

The distributed active sensors embedded in or bonded to the panel are located so that the amplitudes of both the first and second modes of the fluttering panel are sensed separately as outputs. Similarly, input signals are fed to the actuators distributed over the surfaces of the panel so as to independently actuate both the first and second modes of the panel. This is a case of a multi-input multi-output nonlinear system, and the analysis presented in Section 4.3 can be applied to the multi-input multi-output active panel undergoing fluttering given in Eq. (4.31) below:

$$\dot{x} = f(x) + g_1(x)u_1 + g_2(x)u_2 \tag{4.53}$$

$$y_1 = h_1(x)$$

$$y_2 = h_2(x) \tag{4.54a,b}$$

where

$$f(x) = \begin{Bmatrix} x_3 \\ x_4 \\ c_{fv}x_2 - c_{k3}x_1 - c_d x_3 - c_{330}x_1^3 - c_{312}x_1x_2^2 \\ -c_{fv}x_1 - c_{k4}x_2 - c_d x_4 - c_{403}x_2^3 - c_{421}x_1^2x_2 \end{Bmatrix}$$

$$g_1(x) = \begin{Bmatrix} 0 \\ 0 \\ b_{31} \\ b_{41} \end{Bmatrix}, \qquad g_2(x) = \begin{Bmatrix} 0 \\ 0 \\ b_{32} \\ b_{42} \end{Bmatrix}$$

and the outputs are:

$$y_1 = h_1(x) = x_1$$

$$y_2 = h_2(x) = x_2$$

From the computed Lie derivatives, we have

$$L_f^2 h_1 = -c_{k3} x_1 - c_{330} x_1^3 + c_{fv} x_2 - c_{312} x_1 x_2^2 - c_d x_3$$

$$L_f^2 h_2 = -c_{fv} x_1 - c_{k4} x_2 - c_{421} x_1^2 x_2 - c_{403} x_2^3 - c_d x_4$$

The vector relative degree, $\{r_1, r_2\} = \{2,2\}$, and the total scalar relative degree is 4.

$$E(x) = \begin{bmatrix} b_{31} & b_{32} \\ b_{41} & b_{42} \end{bmatrix} \tag{4.55}$$

The coordinate transformations of the x coordinates in terms of the new coordinates ξ are given as:

$$x_1 = \xi_1^1$$
$$x_2 = \xi_1^2$$
$$x_3 = \xi_2^1$$
$$x_4 = \xi_2^2$$

The Jacobian matrices of the transform and inverse transform are given below, and they are nonsingular and well defined.

$$\left| \frac{d\Phi}{dx} \right| = -1$$

Hence, the coordinate transformation is global diffeomorphism.

The original system dynamics given in Eq. (4.31) are represented in the new coordinates as:

$$\begin{Bmatrix} \dot{\xi}_1^1 \\ \dot{\xi}_2^1 \\ \dot{\xi}_1^2 \\ \dot{\xi}_2^2 \end{Bmatrix} = \begin{Bmatrix} \xi_2^1 \\ -c_{k3}\xi_1^1 - c_{330}(\xi_1^1)^3 + c_{fv}\xi_1^2 - c_{312}\xi_1^1(\xi_1^2)^2 - c_d\xi_2^1 \\ \xi_2^2 \\ -c_{k4}\xi_1^2 - c_{403}(\xi_1^2)^3 - c_d\xi_2^2 - c_{fv}\xi_1^1 - c_{421}(\xi_1^1)^2\xi_1^2 \end{Bmatrix} + \begin{Bmatrix} 0 \\ b_{31} \\ 0 \\ b_{41} \end{Bmatrix} u_1 + \begin{Bmatrix} 0 \\ b_{32} \\ 0 \\ b_{42} \end{Bmatrix} u_2 \tag{4.56}$$

for reference trajectories:

$$\dot{\xi}_2^1 = v_1$$

$$\dot{\xi}_2^2 = v_2 \qquad (4.57a,b)$$

where the new control input are

$$v_1 = b_1(\xi) + a_1^1(\xi)u_1(t) + a_2^1(\xi)u_2(t)$$

$$v_2 = b_2(\xi) + a_1^2(\xi)u_1(t) + a_2^2(\xi)u_2(t)$$

The state feedback control laws are formulated so that the nonlinearities in eq. (4.56) are cancelled, and they are given as

$$u_1 = \frac{b_{42}}{\Delta}\left(v_1 - \left(-c_{k3}\xi_1^1 - c_{330}(\xi_1^1)^3 + c_{fv}\xi_1^2 - c_{312}\xi_1^1(\xi_1^2)^2 - c_d\xi_2^1\right)\right) + \frac{b_{32}}{\Delta}\left(-v_2 - c_{k4}\xi_1^2 - c_{403}(\xi_1^2)^3 - c_d\xi_2^2 - c_{fv}\xi_1^1 - c_{421}(\xi_1^1)^2\xi_1^2\right) \qquad (4.58a)$$

$$u_2 = \frac{b_{41}}{\Delta}\left(-v_1 - c_{k3}\xi_1^1 - c_{330}(\xi_1^1)^3 + c_{fv}\xi_1^2 - c_{312}\xi_1^1(\xi_1^2)^2 - c_d\xi_2^1\right) + \frac{b_{31}}{\Delta}\left(v_2 - \left(-c_{k4}\xi_1^2 - c_{403}(\xi_1^2)^3 - c_d\xi_2^2 - c_{fv}\xi_1^1 - c_{421}(\xi_1^1)^2\xi_1^2\right)\right) \qquad (4.58b)$$

$$\Delta = b_{31}b_{42} - b_{32}b_{41}$$

The feedback linearized models, which are two fully decoupled second-order dynamic system given in Eq. (4.59) and Eq. (4.60) become

Mode 1:

$$\dot{\xi}_1^1 = \xi_2^1$$

$$\dot{\xi}_2^1 = v_1, \qquad (4.59a)$$

$$\text{where } v_1 = -k_0^1\xi_1^1 - k_1^1\xi_2^1 \text{ by pole placements} \qquad (4.59b)$$

The first output

$$y_1 = \xi_1^1$$

Mode 2:

$$\dot{\xi}_1^2 = \xi_2^2$$

$$\dot{\xi}_2^2 = v_2\,, \tag{4.60a}$$

$$\text{where } v_2 = -k_0^2\xi_1^2 - k_1^2\xi_2^2 \text{ by pole placements} \tag{4.60b}$$

The second output

$$y_2 = \xi_1^2$$

Once again, just as in the previous two sections, the new inputs are chosen so that each resulting mode is asymptotically stable. One can observe that there is no internal dynamics when the original multi-input multi-output nonlinear system is employed because the original system given in Eq. (4.53) and Eq. (4.54) is fourth-order with two control inputs having total scalar relative degree of 4, that is, $r = n$.

5. NUMERICAL SIMULATIONS

A simply supported rectangular panel with two piezoelectric layers segmented into rectangular patches is used for the numerical simulations. The panel is an aluminum panel, while the piezoelectric layers are lead zirconate titanate (PZT) ceramics. It is assumed that the PZT patches are perfectly and symmetrically bonded to the rectangular aluminum panel to form an active panel. The geometry and the material properties of the intelligent panel are given in Table 5.1.

The mathematical model of the active panel dynamics is presented in Chapter 3. This model, which is represented as a set of modal nonlinear differential equations, accounts for various forces acting on the intelligent panel including aerodynamic loads, externally applied in-plane loads and electrical displacements. The aerodynamic loads, which are represented by the nondimensional dynamic pressures, induce instability of the intelligent panel resulting in panel flutter with associated limit cycle motions. The electrical displacements produced the actuation of the piezoelectric ceramics that are used to suppress the limit cycle motions through output feedback linearizing control developed in this research. The feedback linearizations transform the nonlinear models to simple Brunovsky canonical forms.

Table 5.1 The geometrical and the material properties of the active panel

	Host layer	Actuator
Material	Aluminum	Lead zirconium titanate
Length (in.)	a : 12.0	x_p : $0.1a$
Width (in.)	b : 12.0	y_p : $0.6b$
Thickness (in.)	h_s : 0.05	h_p : 0.005
Mass density (Ib-sec^2/in^4)	ρ_s : 0.2588×10^{-3}	ρ_p : 0.7101×10^{-3}
Young's modulus (psi)	E_s : 10.4×10^{6}	E_p : 9.0×10^{6}
Poisson's ration	ν_s : 0.3	ν_p : 0.3
Charge constant (in./v)	-	d_{31} : -7.478×10^{-9}
Charge constant (in./v)	-	d_{32} : -7.478×10^{-9}
Charge constant (in./v)	-	d_{36} : 0
Coercive Field (v/in.)	-	$e_{\max}$: 15243

A Runge-Kutta integration scheme was used to simulate the modal nonlinear models. The integration time step was chosen to be about one tenth of the smallest period of the normal modes, that is, $\Delta\tau = 0.0015$. Initial conditions were chosen arbitrarily, but the same values were used for all the simulations. Generally, any chosen initial conditions still result in limit cycle motions. Panel flutter with associated limit cycle motions were obtained by the integrations, and the suppression of these limit cycle motions were demonstrated by activating the controllers at specified time. Two linear normal modes were used to model panel flutter in this research. The calculations were conducted in time domain.

The PZT patches were used as both actuators and sensors simultaneously. These patches were activated independently, so that the motions of the panel were sensed and actuated at desired locations on its surfaces, therefore, the active panel was controlled by single input and multi-input signals through these actuators. Three cases were considered: the first case was when the first mode was sensed as output signal, and it was shown in Fig. (5.1), the second case was when the output signal of the second mode was sensed as shown in Fig. (5.2), and the third case was when both the first and the second modes were sensed as shown in Fig. (5.3). The output signals were modified and fed back through the actuators as shown above.

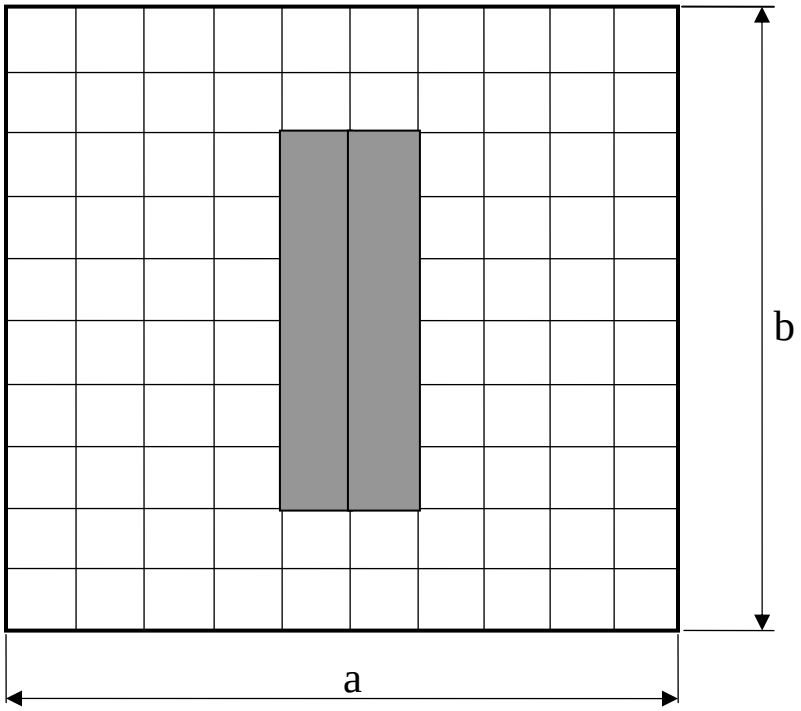

Fig. 5.1 A simply-supported plate showing the actuators for the first mode

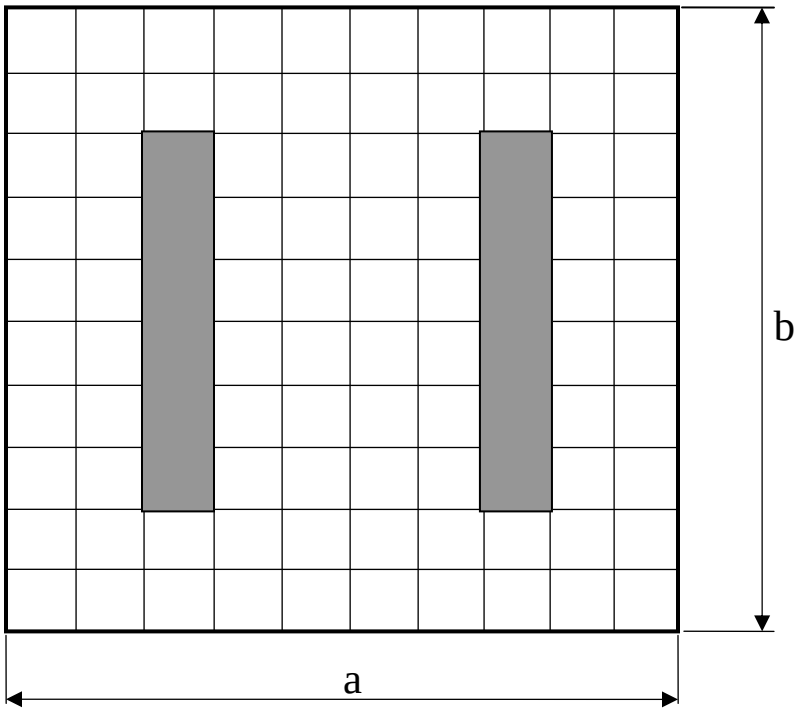

Fig. 5.2 A simply-supported plate showing the actuators for the second mode

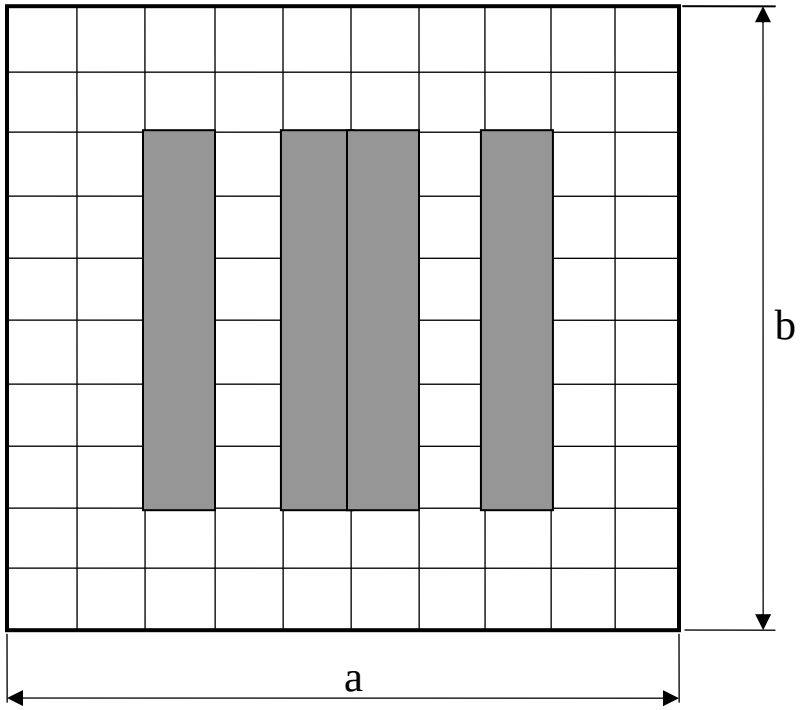

Fig. 5.3 A simply-supported plate showing the actuators for first and second modes

5.1 Limit-Cycle Motion of the Panel Flutter

The panel flutter is induced by the aerodynamic pressure on one side of the panel. The critical dynamic pressure is calculated by eigenvalue analysis of the linear system, and this is given by its open-loop roots.

Based on the panel dynamics, the aerodynamic pressure affects both the damping terms and the flow coupling terms in the system. The panel exhibits free oscillations when there is no aerodynamic pressure, and there are no other damping and nonlinear effects in the system. Linear eigenvalue analysis shows that it has purely imaginary eigenvalues. The application of aerodynamic pressure introduces both damping and flow coupling terms, so the panel exhibits damped oscillations, and the system has complex eigenvalues with negative real parts, which lead to the decay of the oscillation of the panel. As the dynamic pressure (λ) is increased, the rate of decay increases until it reaches a critical point, at which there exists a pair of purely imaginary eigenvalues, with the other eigenvalues having negative real parts, and this signifies the onset of panel flutter. At this critical point, the dynamic pressure is called the critical dynamic pressure ($\lambda_{cr} = 385$), and the system becomes critical. Beyond this critical point, the pair of purely imaginary eigenvalues becomes eigenvalues with positive real parts, the motion of the panel diverges, and the system becomes unstable by linear analysis and the amplitude of the panel deflection diverges, but the structural nonlinearity due to the effect of the in-plane stretching forces becomes significant and acts as a restoring force, and the amplitude stays at a certain value with limit-cycle motion of the panel, and fluttering of the panel is sustained.

In [54], six linear normal modes were used for numerical analysis, but the critical dynamic pressures using two to six linear normal modes were presented. While the critical dynamic pressure obtained is 515 for six linear normal modes, it is 385 for two normal linear modes. Although, four or six linear modes are required for obtaining a converged limit-cycle amplitude and frequency [13], several research works have been presented with two normal modes [10, 16, 17, 21, 27].

The model was run with the dynamic pressure set to 1,500, which is about 3.9 times the critical dynamic pressure. An aerodynamic damping coefficient of $c_a = 0.01$ was used. Fig. (5.4) shows the deflection profile of the mid-span of the panel in the flow direction at a specific instant of time. The position of the maximum deflection, $w_{\max}$, of the panel is at about 68.5% of the panel length. The time history of the deflection of the position of maximum deflection is shown in Fig. (5.5a), and it reflects the panel flutter that is taking place, and the existence of limit cycle motion is shown in Fig. (5.5b).

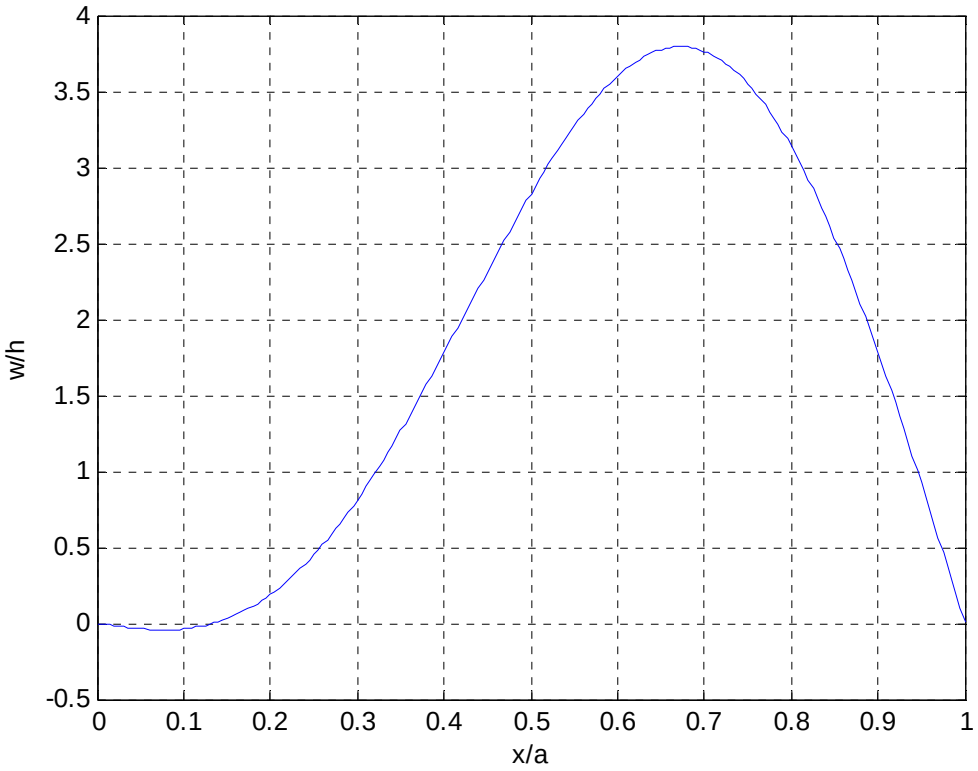

Fig. 5.4 Panel deflection of a simply-supported plate at the mid-span in the flow direction

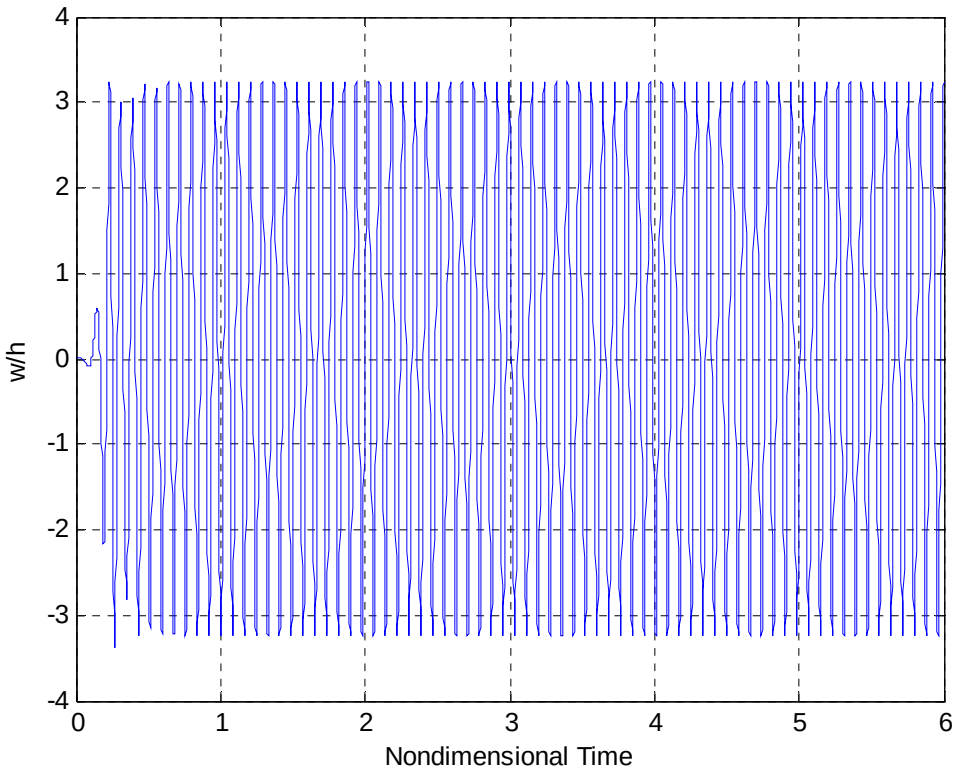

Fig. 5.5 Time history of uncontrolled panel deflection, at $\lambda = 1500$ and $R_x^m = 0$.

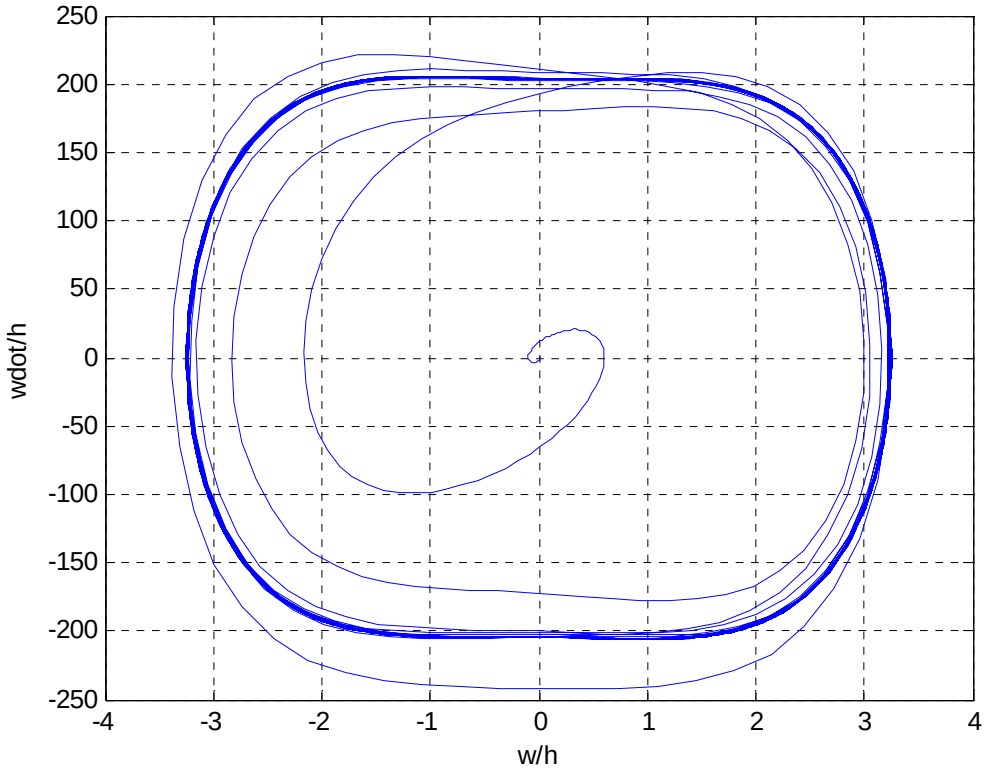

Fig. 5.6 Phase plot of uncontrolled panel deflection, at $\lambda = 1500$ and $R_x^m = 0$.

5.2 Suppression of Panel Flutter due to Aerodynamic Load only

At a dynamic pressure, $\lambda = 1500$, panel flutter limit cycle motions are obtained first, and then the controllers are activated to suppress them at a selected time. In order to suppress the panel flutter limit cycle motion, a closed-loop system with feedback linearization controllers developed in this research were used. The linearized systems in the transformed coordinates were in canonical controllable forms; hence, the pole-placement techniques were used to select the control gains, such that the roots of the closed-loop systems were entirely in the left half of the complex plane, hence, the feedback linearized system becomes asymptotically stable. The control inputs are the electric fields, generated by the electric potentials applied on the PZT patches. There are maximum allowable electric fields, above which depolarization of the piezoelectric property takes place, but that is not one of the objective of this research.

The PZT patches sense the magnitude of the output of the first mode, second mode, or both first and second modes of the limit cycle motions of the panel flutter. These are the three cases shown in Fig. (5.1-3). In each case, the selected output is fed to the controllers that modify the signals, and is fed back to the actuators, and this actuates the panel so that the magnitudes of limit cycles are suppressed, until the sensor senses no deflection of the panel from the equilibrium.

For the three cases, plots of the zero dynamics, plots of the time histories for the panel at the position of maximum deflection, plots of the normalized control inputs, and phase plots are shown in Fig. (5.7 – 14). The zero dynamics for the single-input nonlinear systems show that they are asymptotically stable. The limit cycle motions are suppressed

and the selected point stabilized at the undeflected point, except for the second case, where the second mode is used as the output, the selected point stabilizes at a new equilibrium. See Fig. (5.10) and Fig. (5.11) for the phase plot of the zero dynamics and plot of time history, respectively. This is confirmed by placing the poles of the closed-loop system at other various locations.

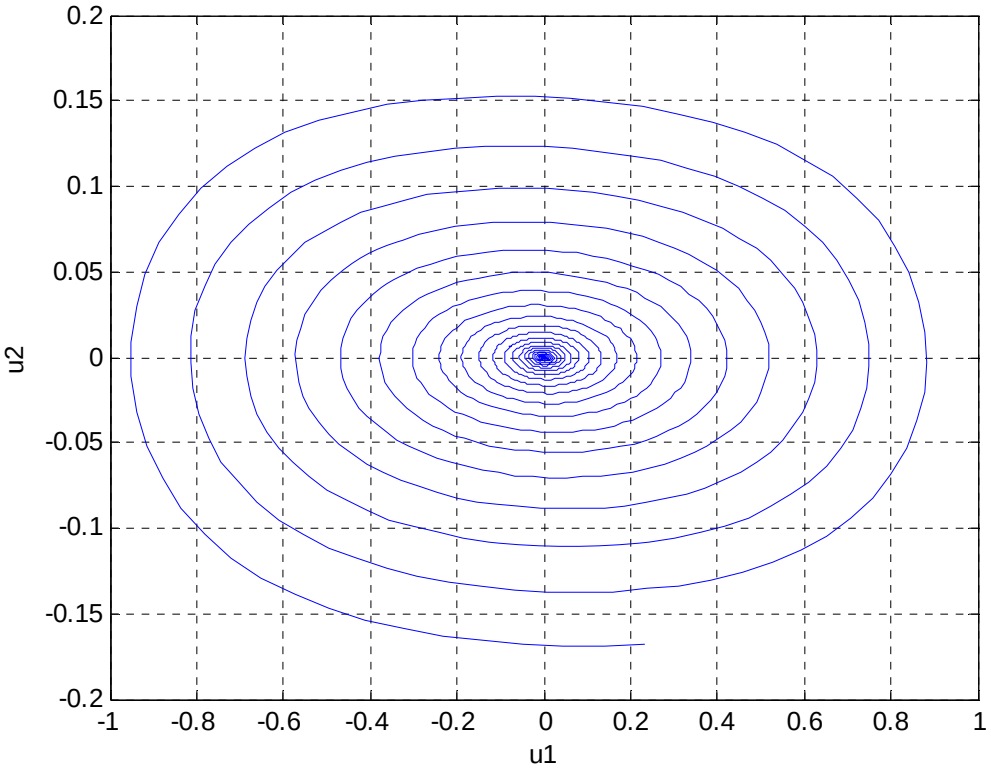

Fig. 5.7 Phase plot of the zero dynamics for the panel at $\lambda = 1500$ and $R_x^m = 0$, using the first mode as the output.

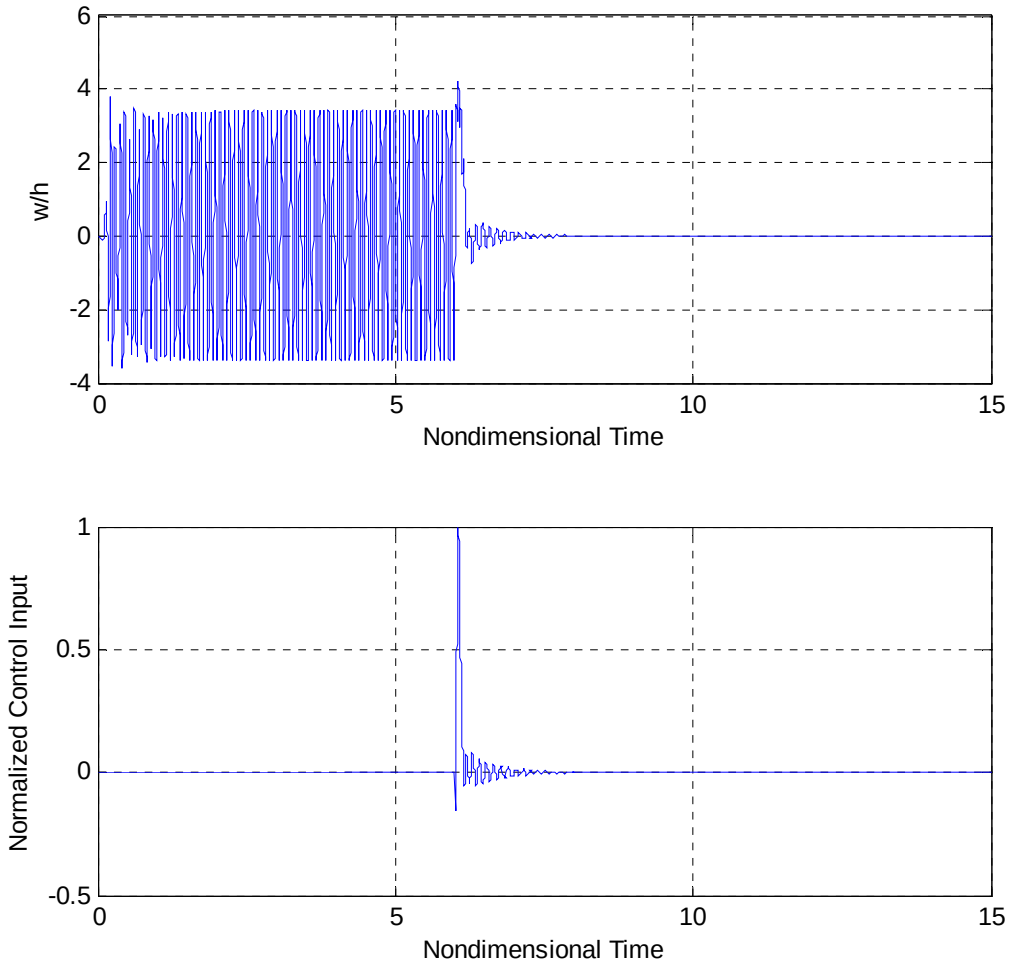

Fig. 5.8 Time history of panel deflection and control effort with feedback linearization controller, at $\lambda = 1500$ and $R_x^m = 0$, using the first mode as the output.

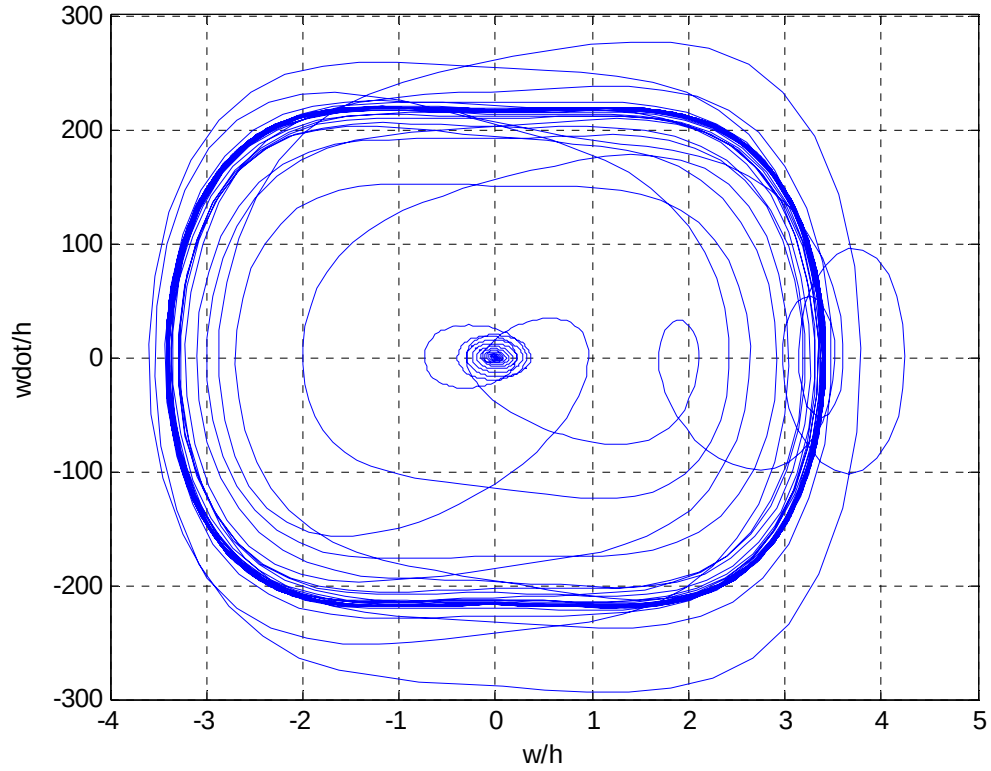

Fig. 5.9 Phase plot of the panel with feedback linearization controller, at $\lambda = 1500$ and $R_x^m = 0$, using the first mode as the output.

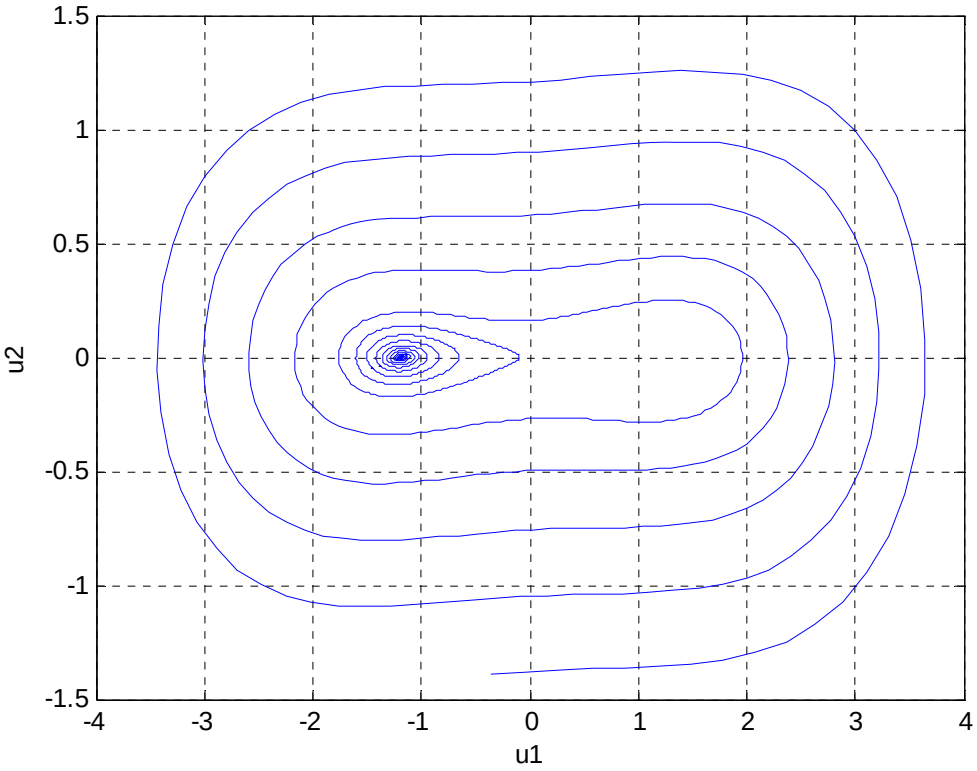

Fig. 5.10 Phase plot of the zero dynamics for the panel at $\lambda = 1500$ and $R_x^m = 0$ shows a new equilibrium, when the second mode is the output.

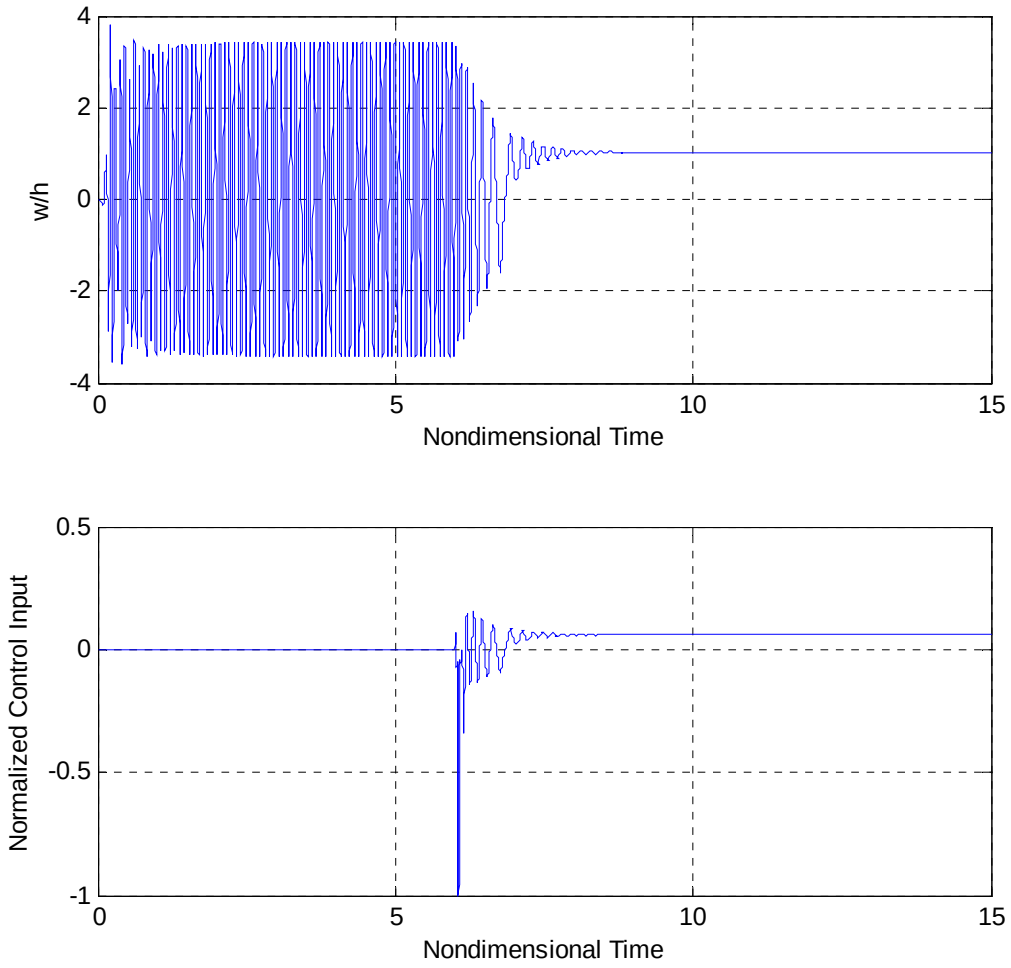

Fig. 5.11 Time history of panel deflection and control effort with feedback linearization controller, at $\lambda = 1500$ and $R_x^m = 0$, using the second mode as the output.

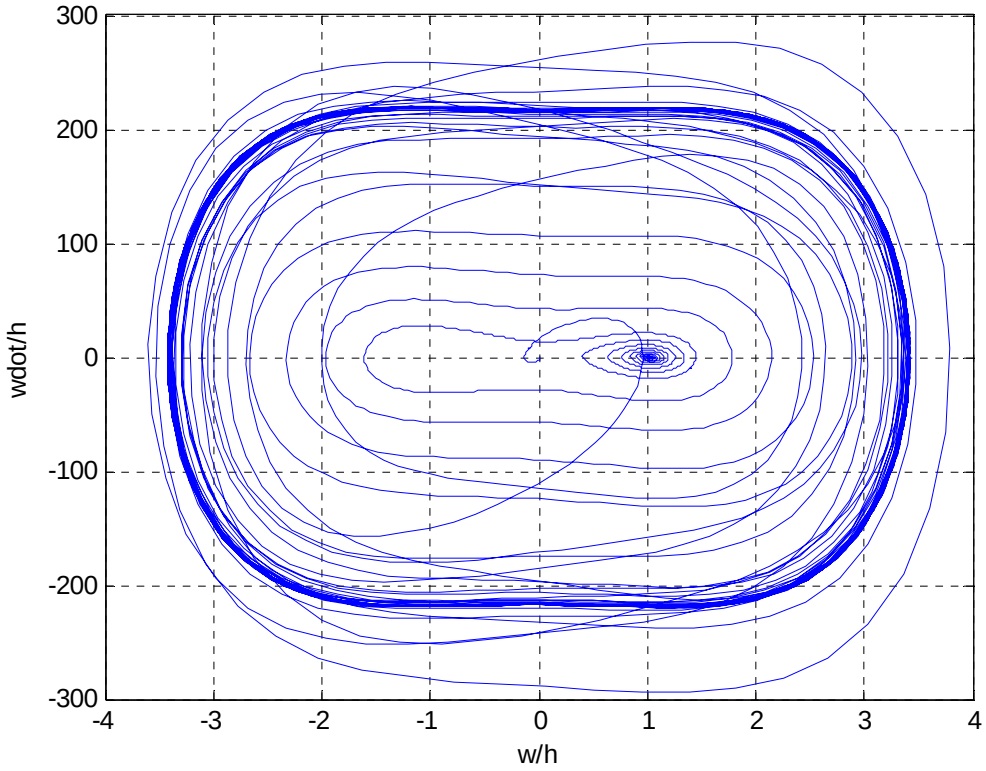

Fig. 5.12 Phase plot of the panel with feedback linearization controller, at $\lambda = 1500$ and $R_x^m = 0$, using the second mode as the output.

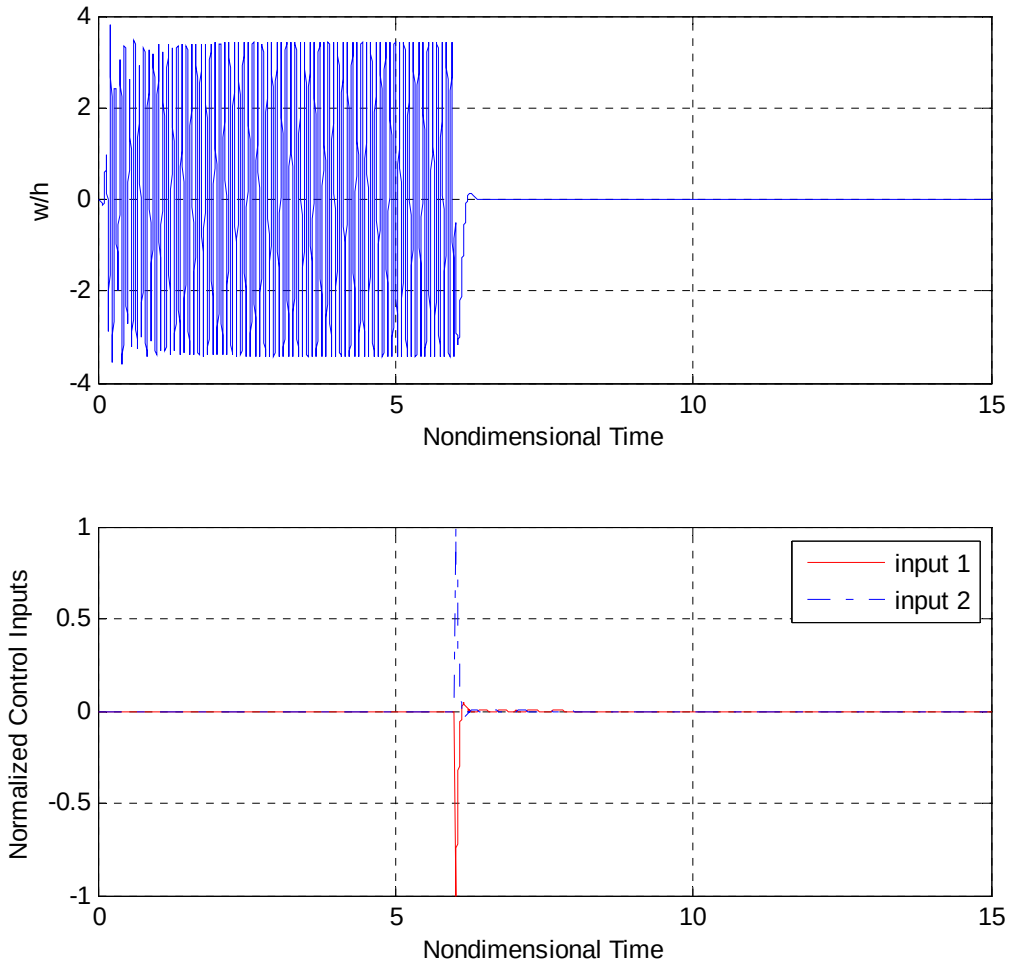

Fig. 5.13 Time history of panel deflection and control efforts with feedback linearization controller, at $\lambda = 1500$ and $R_x^m = 0$, using first and second modes as outputs.

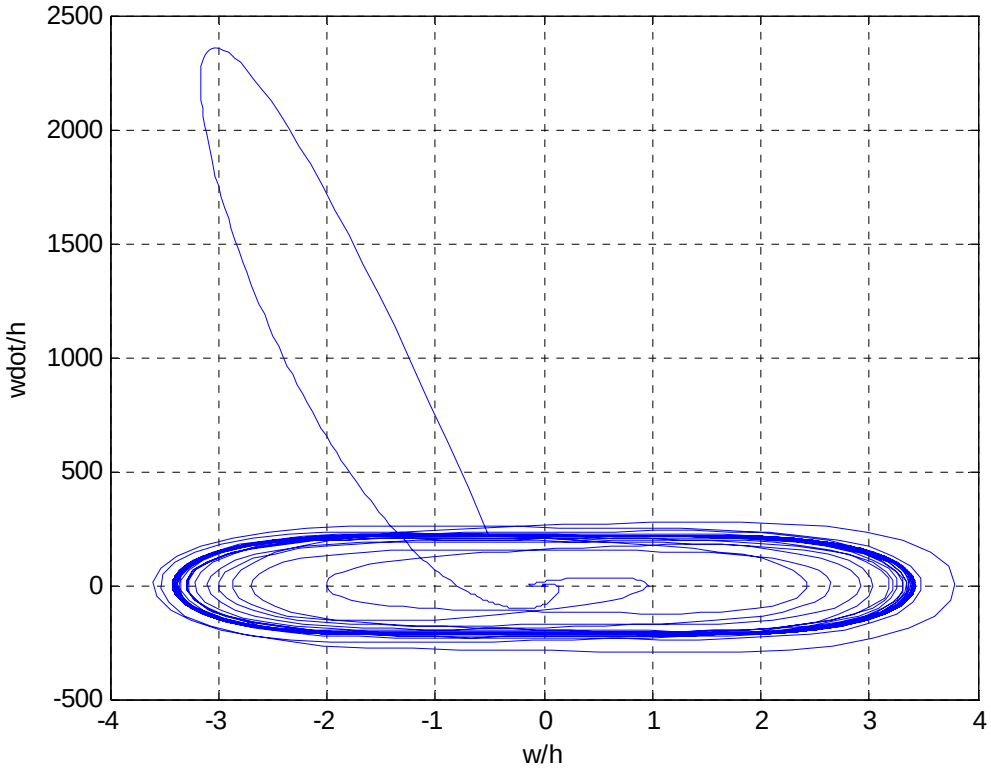

Fig. 5.14 Phase plot of the panel with feedback linearization controller, at $\lambda = 1500$ and $R_x^m = 0$, using first and second modes as outputs.

5.3 Suppression of Panel Flutter due to Combined Aerodynamic and Externally Applied In-plane Forces

In this section, it is considered that an externally applied in-plane load is on the panel with the aerodynamic load. The latter is set at a dynamic pressure, $\lambda = 380,$ and the former is set at a normalized in-plane load $R_x = -\pi^2,$ that is, a compressive load. At this dynamic pressure, without the externally applied load, the panel is stable, that is, there is no panel flutter, but the applied in-plane load causes the panel to flutter at lower dynamic pressure. For this condition, the critical dynamic pressure λ_{cr} is 325. In order to suppress panel flutter limit cycle motion due to these conditions, the same controllers with the same closed-loop roots pole placed as in the previous section are employed. These poles can be placed in different places for better quality of suppression.

The panel flutter in each case is suppressed. Plots of the zero dynamics, plots of the time histories, plots of the normalized control, and the phase plots are shown in Fig. (5.15-22). The time histories show that the point of maximum deflection stabilizes at the undeflected point, except for the second case again, where the second mode is used as the output. For the second case, the selected point stabilizes at a new equilibrium, although this is not revealed in Fig. (5.16), but it can be observed with higher value of dynamic pressure.

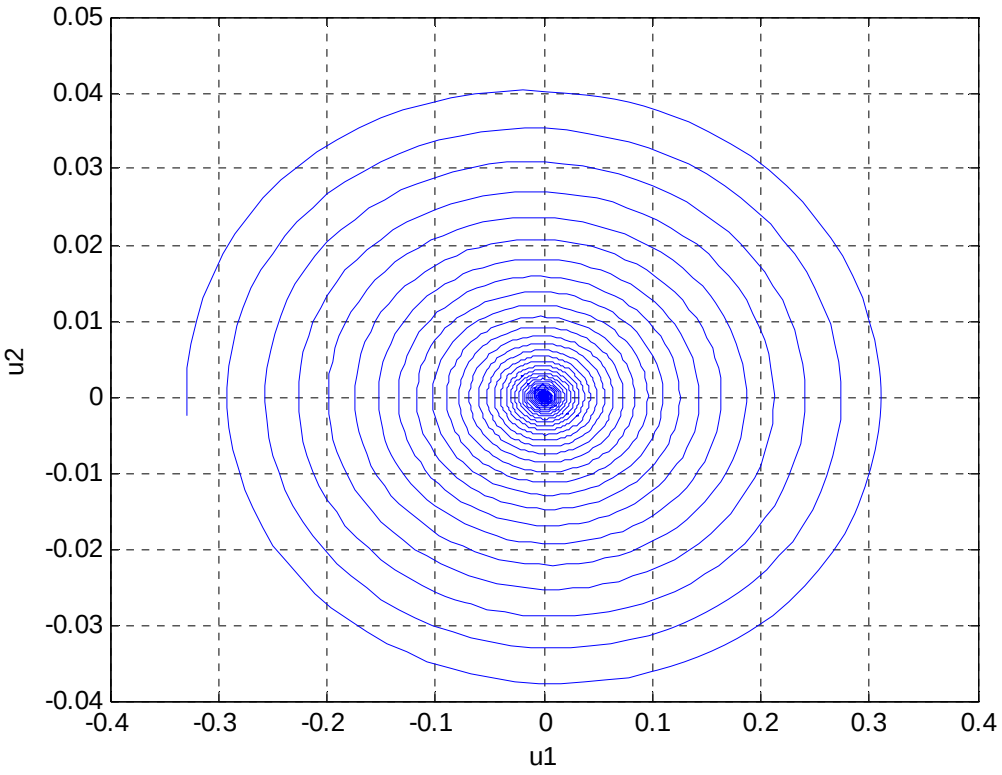

Fig. 5.15 Phase plot of the zero dynamics for the panel at $\lambda = 380$ and $R_x^m = -\pi^2$, using the first mode as the output.

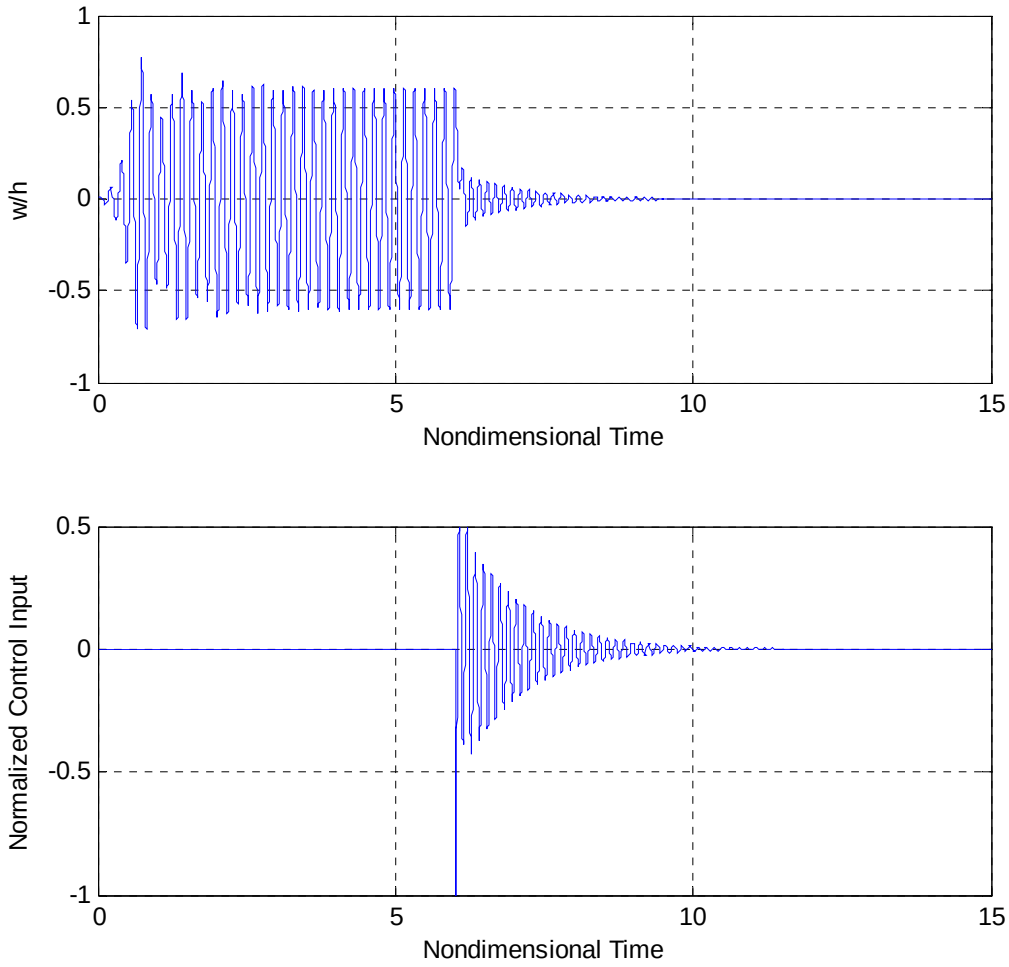

Fig. 5.16 Time history of panel deflection and control effort with feedback linearization controller, at $\lambda = 380$ and $R_x^m = -\pi^2$, using the first mode as the output.

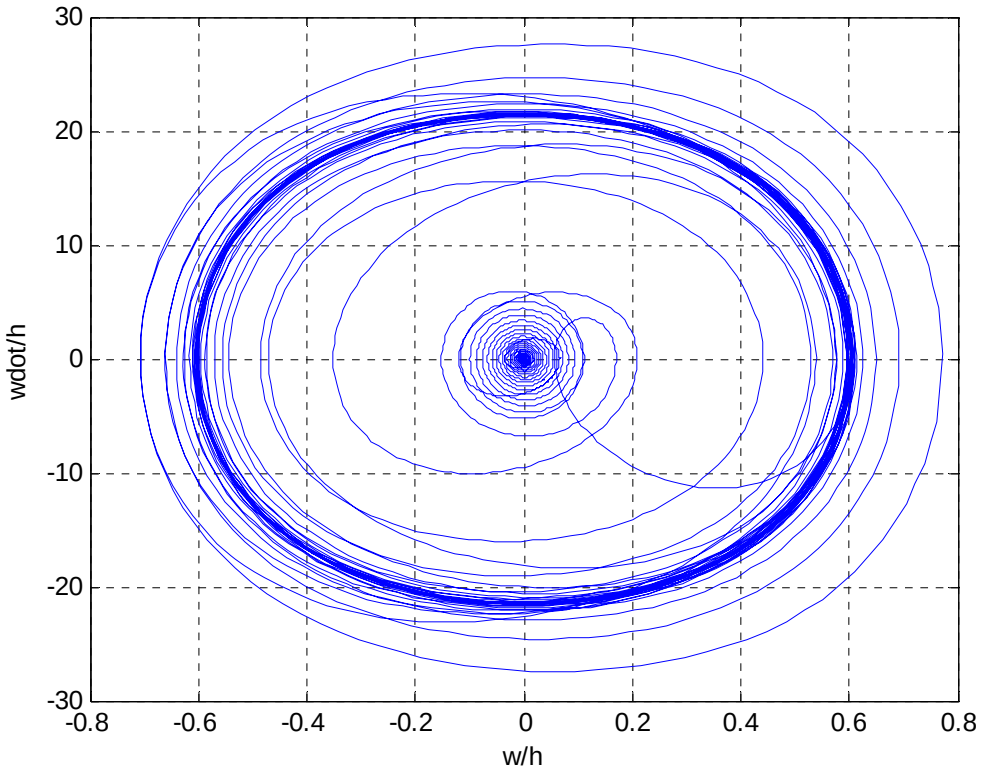

Fig. 5.17 Phase plot for the panel with feedback linearization controller, at $\lambda = 380$ and $R_x^m = -\pi^2$, using the first mode as the output.

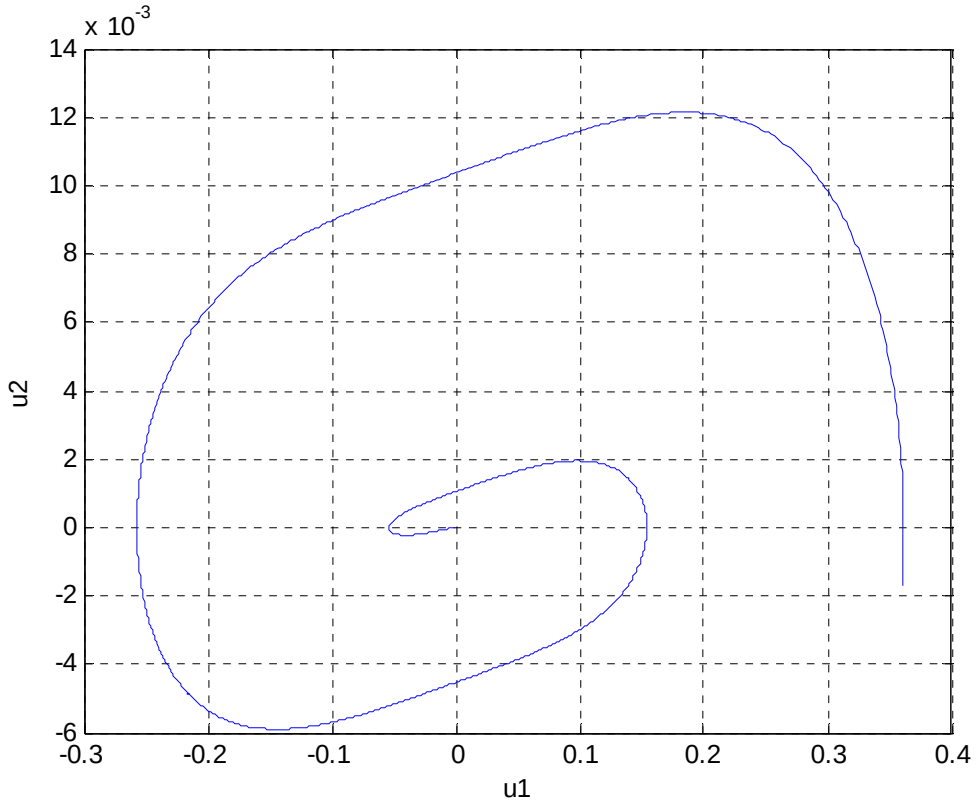

Fig. 5.18 Phase plot of the zero dynamics for the panel at $\lambda = 380$ and $R_x^m = -\pi^2$ shows a new equilibrium, when the second mode is the output.

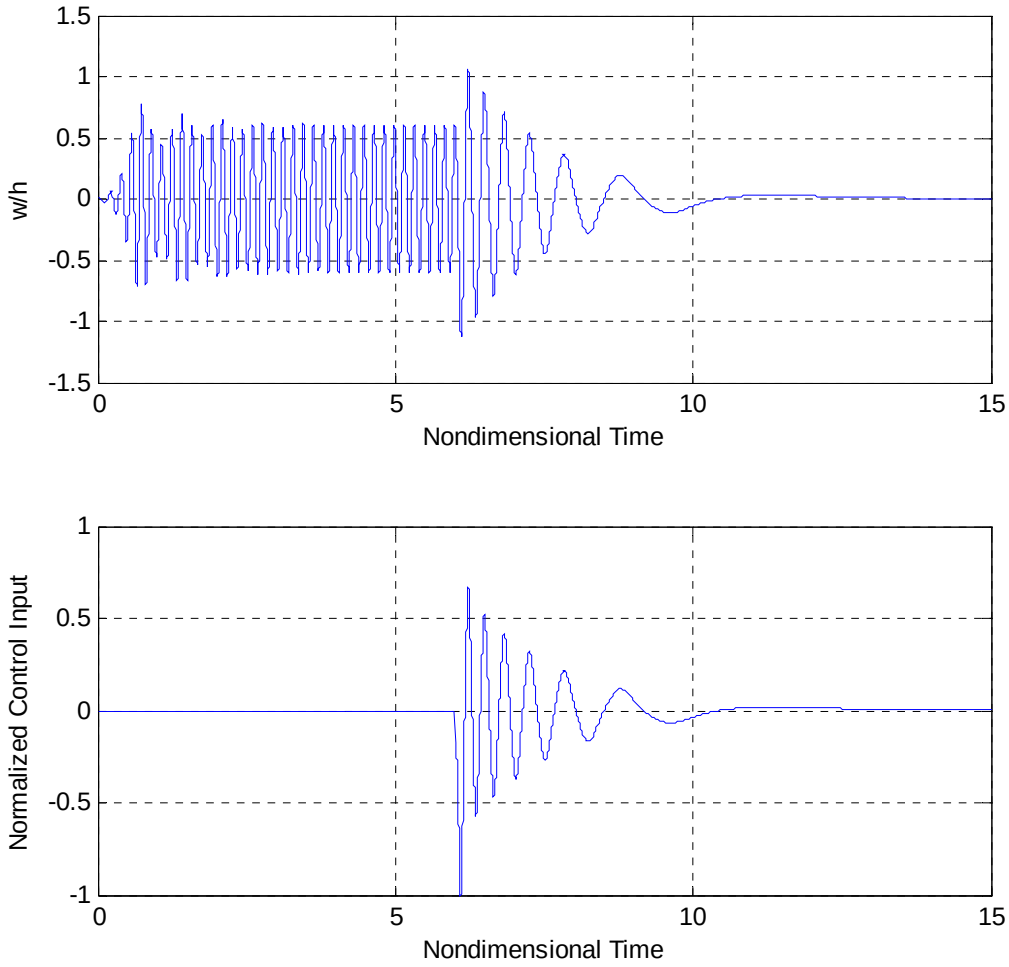

Fig. 5.19 Time history of panel deflection and control effort with feedback linearization controller, at $\lambda = 380$ and $R_x^m = -\pi^2$, using the second mode as the output.

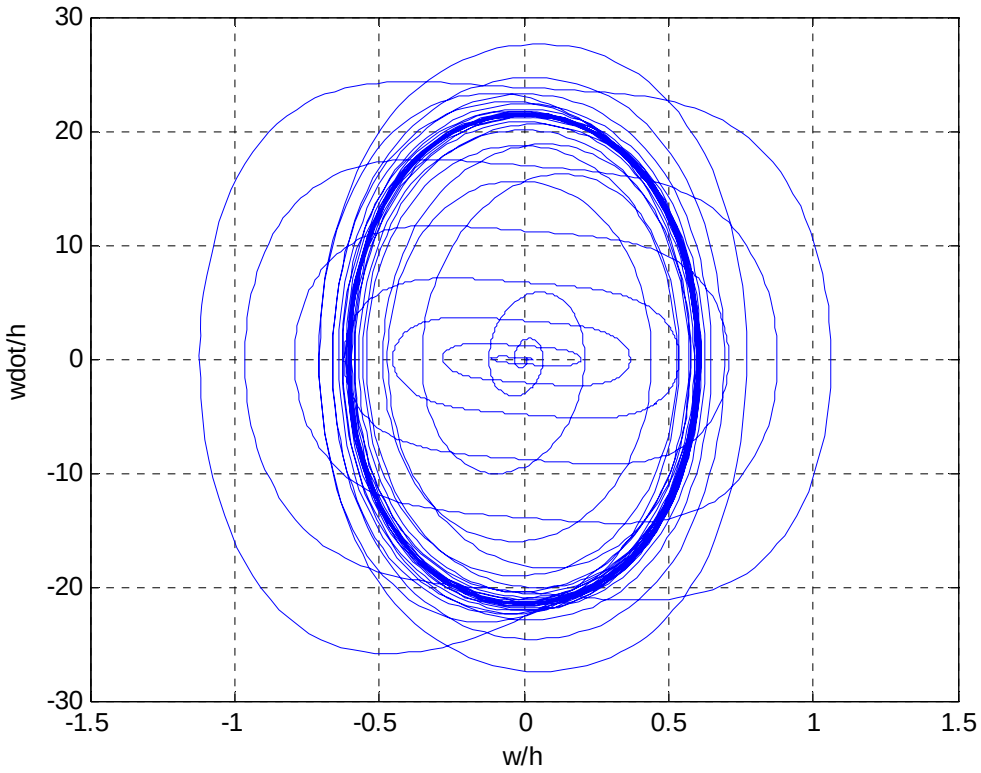

Fig. 5.20 Phase plot for the panel with feedback linearization controller, at $\lambda = 380$ and $R_x^m = -\pi^2$, using the second mode as the output.

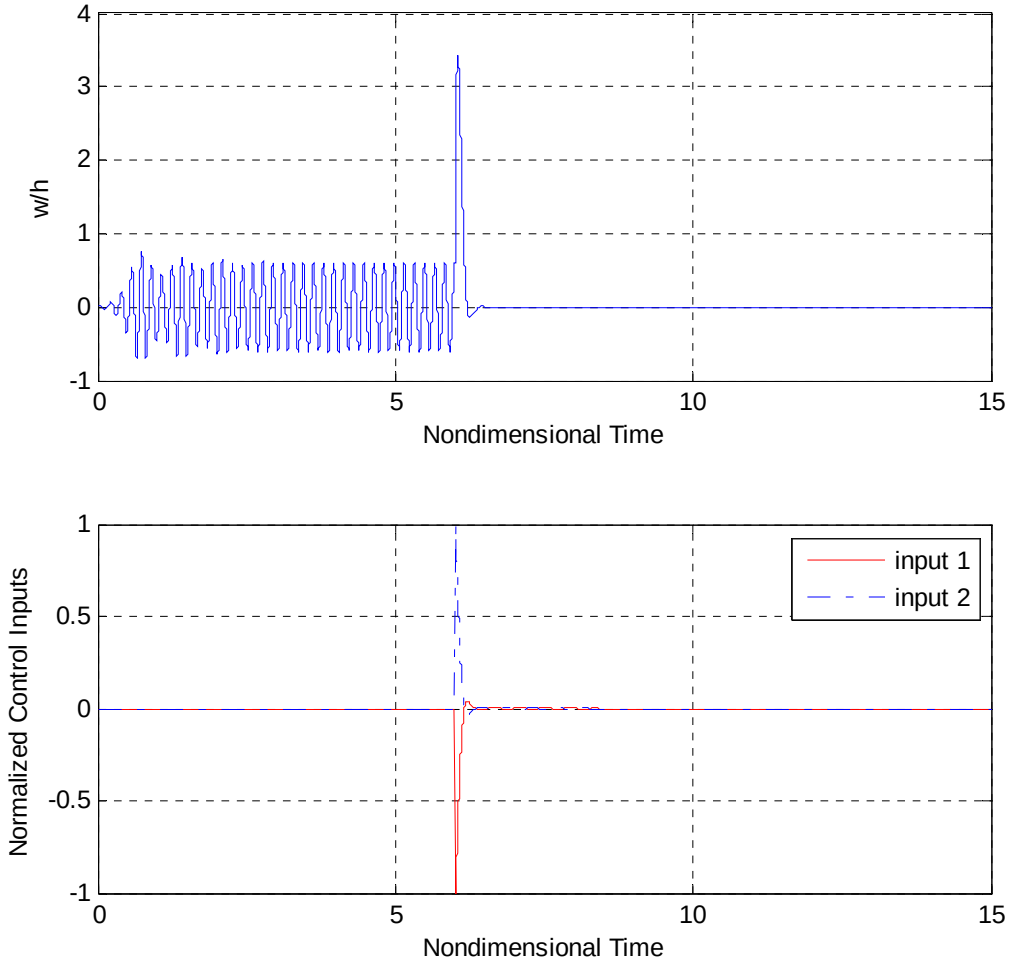

Fig. 5.21 Time history of panel deflection and control efforts with feedback linearization controller, at $\lambda = 380$ and $R_x^m = -\pi^2$, using first and second modes as outputs.

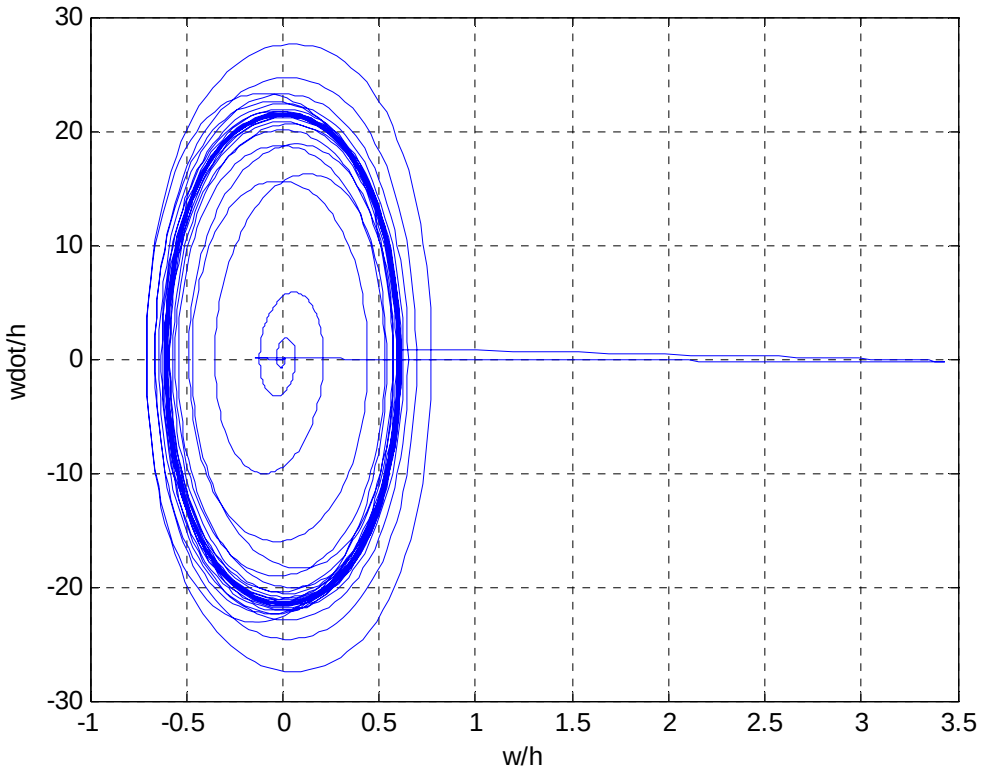

Fig. 5.22 Phase plot for the panel with feedback linearization controller, at $\lambda = 380$ and $R_x^m = -\pi^2$, using first and second modes as outputs.

6. CONCLUSIONS AND RECOMMENDATIONS

6.1 Conclusions

Feedback linearization is based on nonlinear control theory, and it has been used in this study to transform the nonlinear panel flutter problem into an equivalent controllable linear problem that can be written in simple Brunovsky canonical form by the chosen outputs. This takes into account the nonlinear characteristics of panel flutter dynamics in the design of nonlinear feedback controllers. Nonlinear feedback control laws are developed and used to cancel the nonlinear dynamics resulting in a linear problem. The pole placement technique is then employed so as to make the states of the feedback linearized model locally asymptotically stable at a given equilibrium.

Using this approach of feedback linearization, nonlinear dynamic equations of an intelligent panel subject to aerodynamic loads with or without externally applied in-plane load are transformed into linear equations in the new coordinates. This intelligent plate has piezoelectric actuators and sensors symmetrically bonded to its surfaces. The piezoelectric actuations of the piezoelectric layers enable the plate to actively respond to external stimuli that cause large deflections and instability resulting in the failure of the panel due to fatigue. With this development, advanced aircraft or vehicles and surfaces in a fluid medium can operate in supersonic environments by the use of this intelligent panel.

The nonlinear dynamic are nonlinear coupled partial differential equations obtained from von Kárman large-deflection plate theory accounting for the structure nonlinearity, and reduced to nonlinear modal equations using two normal modes by Galerkin's method with modal expansion. The nonlinear modal equations are transformed to state-space format, using the amplitudes of the modes and their derivatives as the states, and presented as a nonlinear control system. Linear panel flutter analyses are carried out to determine the critical dynamic pressures λ_{cr} at which there are onsets of panel flutter limit cycle motions. At dynamic pressures above the critical dynamic pressure, limit cycle motions are considered large, therefore nonlinear panel flutter analysis is employed. The piezoelectric actuation of the active panel drives the actuators to suppress the panel flutter associated limit cycle motions, and it is carried out by the piezoelectric bending moment generated by the electric field, which is considered as the control input, and it is applied on the actuators.

In selecting the output to linearize the nonlinear control system, three outputs are considered, and these are the first mode, second mode, and both first and second modes. These are three cases for which numerical simulations are carried out. The closed-loop systems for the first two cases are classified as single-input single-output nonlinear systems, and only partial feedback linearization is carried out, therefore, there are internal dynamics, which are established to be locally asymptotically stable. In the third case, the closed-loop system is classified as multi-input multi-output nonlinear system, and full feedback linearization is carried out, thus, in this case, there are no internal dynamics.

The closed-loop systems for the three cases are numerically simulated at much higher dynamic pressures than the critical dynamic pressures so that limit-cycle motions

are generated. The simulated systems show that the closed-loop systems based on the controllers effectively suppress panel flutter limit cycle motions with the generated piezoelectric bending actuations as control inputs. Therefore, with the feedback linearization controllers developed, the limit cycle motion of panel flutter can be completely suppressed if the controller gains are carefully selected.

The flutter free dynamics are also achieved if the actuators are activated before the critical dynamic pressure is reached, therefore, the dynamic pressure of the panel can be allowed to exceed the critical dynamic pressure λ_{cr} without flutter. This approach is practically more feasible than the suppression of limit-cycle motions, when aircraft wing or air vehicle surface is loaded with aerodynamic loads.

6.2 Recommendations

Based on the studies carried out in this research, there are ample opportunities to improve and extended the effort here, and some of these are highlighted below:

The technique used in this study can be used to linearize the nonlinear dynamics for panel flutter reduced to nonlinear modal equations based on Galerkin's method with modal expansions using five or six linear modes.

In this research, feedback linearization has shown a promising opportunity to develop a flutter free intelligent panel, and this provides tremendous opportunity for aeroservoelasticians in terms of research and development of aircraft wings with superior performance in a supersonic environment. Therefore, it is necessary that a physical system be built, with the analysis in this study and other future analytical works used as benchmarks.

In the present effort, the maximum allowable electric field that can lead to depolarization of the piezoelectric ceramics is not considered as a limitation, but for practical system, it is. Therefore, optimal control technique can used to design the controllers for the feedback linearized system.

The mathematical model of panel flutter is idealistic, and the actual system possesses uncertainties, therefore, there is a need to compensate for the uncertainties in the system by designing adaptive and robust controllers.

REFERENCES

[1] Kuo, C. C., Morino, L., and Dungundji, J., "Perturbation and Harmonic Balance for Treating Nonlinear Panel Flutter," *American Institute of Aeronautics and Astronautics Journal*, Vol. 10, No. 11, 1972, pp. 1479-1484.

[2] Y.C. Fung, *An Introduction to the Theory of Aeroelasticity*, Dover Publications, Inc., 1955 (reprinted by Dover 1993).

[3] Jordan, P. F., "The Physical Nature of Panel flutter," *Aero Digest*, February 1956, pp. 34-38.

[4] Bisplinghoff, R. L. and Ashley, H., *Principles of Aeroelasticity*, John Wiley, 1962, p. 419.

[5] Bailey, T. B. and Hubbard, J. E., Jr., "Distributed Piezoelectric Polymer Active Vibration Control of a Cantilever Beam," *Journal of Guidance, Control, and Dynamics*, Vol. 8, No. 5, 1985, pp. 605-611.

[6] Crawley, E. F. and Louis, J. de, "Use of Piezoelectric Actuators as Elements of Intelligent Structures," *American Institute of Aeronautics and Astronautics Journal*, Vol. 25, No. 10, 1987, pp. 1373-1385.

[7] Moon, S.H., Chwa, D., and Kim, S. J., "Feedback Linearization Control for Panel Flutter Suppression with Piezoelectric Actuators," *American Institute of Aeronautics and Astronautics Journal*, Vol. 43, No. 9, 2005, pp. 2069-2073.

[8] Gray, C. E., Jr. and Mei, C., "Large Amplitude Finite Element Flutter Analysis of Composite Panels in Hypersonic Flow," *Proceedings of the American Institute of Aeronautics and Astronautics Journal Dynamics Specialist Conference*, Dallas, TX, April 16-17, 1992, pp. 492-512. See also American Institute of Aeronautics and Astronautics Journal, Vol. 31, No. 6, 1993, pp. 1090-1099.

[9] Hedgepeth, J. M., "Flutter of Rectangular Simply Supported Panels at High Supersonic Speeds," *Journal of the Aeronautical Science*, Vol. 24, No. 8, Aug. 1957, pp. 563-573, and p. 586.

[10] Dugunji, J., "Theoretical Considerations of Panel Flutter at High Supersonic Mach Numbers," *American Institute of Aeronautics and Astronautics Journal*, Vol. 4, No. 7, 1966, pp. 1257-1266.

[11] Dowell, E. H. and Voss, H. M., "Theoretical and Experimental Panel Flutter Studies in the Mach Number Range 1.0 to 5.0," *American Institute of Aeronautics and Astronautics Journal*, Vol. 3, No. 12, 1965, pp. 2292-2304.

[12] Cunningham, H. J., "Flutter Analysis of Rectangular Panels Based on Three-Dimensional Supersonic Unsteady Potential Flow," NASA TRR-256, Feb. 1967.

[13] Dowell, E. H., "Nonlinear Oscillations of a Fluttering Plate," *American Institute of Aeronautics and Astronautics Journal*, Vol. 4, No. 7, 1966, pp. 1267-1275.

[14] Fung, Y. C., "The Flutter of a Buckled Plate in a Supersonic Flow," AFSOR TN 55-237, 1955, Guggenheim Aeronautical Lab., California Institute of Technology, Pasadena, Calif.

[15] Bolotin, V. V., *Nonconservative Problems of the Theory of Elastic Stability*, The Macmillan Company, New York, 1963, pp. 274-312.

[16] Fralich, R. W., "Postbuckling Effects on the Flutter of Simply Supported Rectangular Panels at Supersonic Speeds," TN D-1615, March 1963, NASA.

[17] Kobayashi, Shigeo, "Flutter of Simply Supported Rectangular Panels in a Supersonic Flow – Two-Dimensional Panel Flutter, I – Simply Supported panel, II – Clamped Panel," *Transaction of Japan Society of Aeronautical and Space Sciences*, Vol. 5, 1962, pp. 79-118.

[18] Librescu, L., "Aeroelastic Stability of Orthotropic Heterogeneous Thin Panels in the Vicinity of the Flutter Critical Boundary, Part I," *Journal de Mecanique*, Vol. 4, No. 1, March 1965, pp. 51-76.

[19] Dowell, E. H., "Nonlinear Oscillations of a Fluttering Plate II," *American Institute of Aeronautics and Astronautics Journal*, Vol. 5, No. 10, 1967, pp. 1856-1862.

[20] Dowell, E. H., "Generalized Aerodynamic Forces on a Flexible Plate Undergoing Transient Motion," *Quarterly of Applied Mathematics*, Vol. 24, No. 4, Jan. 1967, pp. 331-338.

[21] Eastep, F. E. and McIntosh, S. C., "The Analysis of Nonlinear Panel Flutter and Response Under Random Excitation or Nonlinear Aerodynamic Loading," *American Institute of Aeronautics and Astronautics/American Society of Mechanical Engineers 11th Structural Dynamics, and Materials Conference*, Denver, CO, April 22-24, 1970, pp. 36-47.

[22] Ventres, C. S., and Dowell, E. H., "Comparison of Theory and Experiment for Nonlinear Flutter of Loaded Plates," *American Institute of Aeronautics and Astronautics Journal*, Vol. 8, No. 11, 1970, pp. 2022-2030.

[23] Dowell, E. H., "Panel Flutter: A Review of the Aeroelastic Stability of Plates and Shells," *American Institute of Aeronautics and Astronautics Journal*, Vol. 8, 1970, pp. 385-399.

[24] Dowell, E. H., *Aeroelasticity of Plates and Shells*, Noordhoff International Publishing, Lyden, The Netherlands, 1975.

[25] Eslami, H., "Nonlinear Flutter and Forced Oscillations of Rectangular Symmetric Cross-Ply and Orthotropic Panels Using Harmonic Balance and Perturbation Methods, "Ph.D. Dissertation, Old Dominion University, Norfolk, VA, 1987.

[26] Yuen, S. W. and Lau, S. L., "Effects of In-Plane Load on Nonlinear Panel Flutter by Incremental Harmonic Balance Method," *American Institute of Aeronautics and Astronautics Journal*, Vol. 29, N0. 9, 1991, pp. 1472-1479.

[27] Morino, L., "A Perturbation Method for Treating Nonlinear Panel Flutter Problems," *American Institute of Aeronautics and Astronautics Journal*, Vol. 7, No. 3, 1969, pp. 405-410.

[28] Ibrahim, R. A. and Orono, P. O., "Stochastic Nonlinear Flutter of a Panel Subjected to Random In-Plane Forces," *International Journal of Non-Linear Mechanics*, Vol. 26, No. 6, 1991, pp. 867-883.

[29] Han, A. D. and Yang, T. Y., "Nonlinear Panel Flutter Using High-Order Triangular Finite Elements," *American Institute of Aeronautics and Astronautics Journal*, Vol. 21, No. 10, 1983, pp. 1453-1461.

[30] Zhou, R. C., Xue, D. Y. and Mei, C., "On Analysis of Nonlinear Panel Flutter at Supersonic Speeds," *Proceedings of the First Industry/University Symposium on HSCT Vehicle*, NC A&T State University, Greensboro, NC, Dec. 4-6, 1994.

[31] Curie, J. and Curie, P., *Comptes Rendus*, Vol. 91, 1880, pp. 294-295.

[32] Crawley, E. F. and Anderson, E. H., "Detailed Models of Piezoceramic Actuation of Beams," *Journal of Intelligent Materials Systems and Structures*, Vol. 1, No. 1, 1990, pp. 4-25.

[33] Hanagud, S., Obal, M. W., and Calise, A. J., "Optimal Vibration Control by Use of Piezoceramic Sensors and Actuators," *Proceedings of the 27th AIAA/ASME/ASCE/AHS Structures*, Structural Dynamics and Materials Conference,

1986, pp.177-185. Also *Journal of Guidance, Control and Dynamics*, Vol. 15, No. 5, pp. 1199-1206.

[34] Im, S. and Atluri, S. N., "Effects of a Piezo-Actuator on a Finitely Deformed beam Subjected to General Loading," *American Institute of Aeronautics and Astronautics Journal*, Vol. 29, No. 12, 1989, pp. 1801-1807.

[35] Wang, T. B. and Rogers, C. A., "Modeling of Finite-Length Spatially-Distributed Induced Stain Actuators for Laminate Beams and Plates," *Journal of Intelligent Material Systems and Structures*, Vol. 2, January 1991, pp. 38-57.

[36] Crawley, E. F. and Lazarus, K. B., 1990, "Induced Strain Actuation of Isotropic and Anisotropic Plates," *American Institute of Aeronautics and Astronautics Journal*, Vol. 28, No. 6, pp. 944-951.

[37] Wang, B. T. and Rogers, C. A., "Laminate Plate Theory for Spatially Distributed Induced Strain Actuators," *Journal of Composite Materials*, Vol. 25, April 1991, pp. 433-452.

[38] Hagood, N. W., Chung, W. H., and von Flotow, A., "Modeling of Piezoelectric Actuator Dynamics for Active Structural Control," *Journal of Intelligent Materials Systems and Structures*, Vol. 1, No. 7, 1990, pp. 327-354.

[39] Burke, S. E. and Hubbard, J. E. Jr., "Active Vibration Control of a Simply-Supported Beam Using a Spatially Distributed Actuator," *IEEE Control Systems Magazine*, Vol. 7, No. 6, 1987, pp. 25-30.

[40] Burke, S. E. and Hubbard, J. E., Jr., "Distributed Transducer Vibration Control of Thin Plates," *Journal of Acoustical Society of America*, Vol. 90, No. 2, 1991, pp. 937-944.

[41] Dimitriadis, E. K., Fuller, C. R., and Rogers, C. A., "Piezoelectric Actuators for Distributed Vibration Excitation of Thin Plates," *Journal of Vibration and Acoustics*, Vol. 113, January 1991, pp. 100-107.

[42] Lee, C. –K. and Moon, F. C., "Modal Sensors/Actuators," *Journal of Applied Mechanics*, Vol. 57, June 1990, pp. 434-441.

[43] Lee, C. –K., "Theory of Laminated Piezoelectric Plates for the Design of Distributed Sensors/Actuators: Part I. Governing Equations and Reciprocal Relationship," *Journal of Acoustical Society of America*, Vol. 87, No. 3, 1990, pp. 1144-1158.

[44] Tanaka, N., Snyder, S. D., and Hansen, C. H., "Distributed Parameter Modal Filtering using Smart Sensors," *Transactions of the American Society of Mechanical Engineers,* Vo. 118, October 1996, pp. 630-640.

[45] Anderson, E. H., and Hagood, N. W., "Simultaneous Sensing and Actuation using Piezoelectric Materials" *SPIE Conference on Active and Adaptive Optical Components*, 1991, SPIE1543-40.

[46] Anderson, E. H., Hagood, N. W., and Goodliffe, J. M., "Self-Sensing Piezoelectric Actuation: Analysis and Application to Controlled Structures," AIAA Paper 92-2465. *Proceedings of the 33rd Structures, Structural Dynamics and Materials Conference*, Dallas, TX, April 1992, pp. 2141-2155.

[47] Dosch, J. J., Inman, D. J., and Garcia, E., "A Self-Sensing Piezoelectric Actuator for Collocated Control," *Journal of Intelligent Materials Systems and Structures*, Vol. 3, No. 1, 1992, pp. 166-185.

[48] Plump, J. M. and Hubbard, J. E., "Nonlinear Control of a Distributed System: Simulation and Experimental Results," *Journal of Dynamic, Systems, Measurement, and Control*, Vol. 109, 1987, pp. 133-139.

[49] Sung, C. K. and Chen, Y. C., "Vibration Control of the Elastodynamic Response of High-Speed Flexible Linkage Mechanisms," *Journal of Vibration and Acoustics*, Vol. 113, January 1991, pp. 14-21.

[50] Chen, S.-H., Wang, Z.-D., and Liu, X. –H., "Active Vibration Control and Suppression for Intelligent Structures," *Journal of Sound and Vibration*, Vol. 200, No. 2, 1997, pp. 167-177.

[51] Joseph, P., "New Strategies in the Control of Linear Dynamic Systems with Periodically Varying Coefficients," Ph.D. Dissertation, Auburn University, Auburn, AL, 1993.

[52] Scott, R. C., and Weisshaar, T. A., "Controlling Panel Flutter Using Adaptive Materials," *Proceedings of 32nd Structures, Structural Dynamics, and Materials Conference*, Baltimore, MD, 1991, pp.2218-2229. American Institute of Aeronautics and Astronautics Journal, Vol. 31, No. 1, 1994, pp. 213-222.

[53] Hajela, P., and Glowasky, R., "Application of Piezoelectric Elements in Supersonic Panel Flutter Suppression," *Proceedings of American Institute of Aeronautics and Astronautics/American Society of Mechanical Engineers/American Society of Electrical Engineers, Aircraft Design Systems and Operations Meeting*, Baltimore, MD, 1991, pp. 1-11. American Institute of Aeronautics and Astronautics Paper No. 91-3191.

[54] Lai, Z., Xue, D.Y., Huang, J.-K. and Mei, C., "Nonlinear Panel Flutter Suppression with Piezoelectric Actuation," *Journal of Intelligent Material Systems and Structures*, Vol. 6, 1995, pp. 274-282.

[55] Heeg, J., "An Analytical and Experimental Investigation of Flutter Suppression via Piezoelectric Actuation," *Proceedings of American Institute of Aeronautics and Astronautics Dynamics Specialist Conference*, Dallas, TX, 1992, pp. 237-247.

[56] Zhou, R.C., Lai, Z., Xue, D.Y., Huang, J.-K. and Mei, C. "Suppression of Nonlinear Panel Flutter with Piezoelectric Actuators using Finite Element Method," *American Institute of Aeronautics and Astronautics Journal*, Vol. 33, 1995, pp. 1098-1105.

[57] Frampton, K. D., Clark, R. L., and Dowell, E. H., "Active Control of Panel Flutter with Piezoelectric Transducers," *Journal of Aircraft*, Vol. 33. No. 4, July – August 1996, pp. 768 – 774.

[58] Lai, Z., Zhou, R. C., Xue, D. Y., Huang, J.-K. and Mei, C., "Suppression of Nonlinear Panel Flutter at Elevated Temperature with Piezoelectric Actuator," *American Institute of Aeronautics and Astronautics/American Society of Mechanical Engineers Adaptive Structures Forum*, LaJolla, CA, April 1993, pp. 3466-3474.

[59] Lai, Zhihong, "Vibration control with piezoelectric actuation applied to nonlinear panel flutter suppression," Ph.D. Dissertation, Old Dominion University, Norfolk, VA, 1994.

[60] Lai, Z., Huang, J. K. and Mei, C., "A Lyapunov-based Nonlinear Control Design in Panel Flutter Suppression with Piezoelectric Actuation," First Industry/University Symposium on HSCT Vehicle, NC A&T, Greensboro, NC, December 1994, pp. 325-330.

[61] Moon, S.H. and Kim, S. J., "Active and Passive Suppression of Nonlinear Panel Flutter Using Finite Element Method," *American Institute of Aeronautics and Astronautics Journal*, Vol. 39, No. 11, November 2001, pp. 2069-2073.

[62] Moon, S.H. and Kim, S. J., "Suppression of Nonlinear Composite Panel Flutter with Active/Passive Hybrid Piezoelectric Networks using Finite Element Method," *Composite Structures*, vol. 59, 2003, pp. 525-533.

[63] Ko, J., Kurdila, A.J., and Strganac, T.W., "Nonlinear control of a Prototypical Wing Section with Torsional Nonliearity," *Journal of Guidance, Control and Dynamics***,** Vol. 20, No. 6, November –December 1997, pp. 1182-1189.

[64] IEEE Standard 176, "Piezoelectricity," IEEE, New York, 1978.

[65] Toupin, R. A., "The Elastic Dielectric," *Journal of Rational Mechanics and Analysis*, Vol. 5, 1956, pp. 849-916.

[66] Tiersten, H. F., *Linear Piezoelectric Plate Vibrations*, Plenum Press, New York, 1969.

[67] Hetnarski, R. B., 1986, *Thermal Stresses I*, Elsevier Science Publishers B. V.

[68] Isidori, A., *Nonlinear Control Systems*, Springer-Verlag, 1989.

[69] Slotine, J. E. and Li, W., *Applied Nonlinear Control*, Prentice Hall, Engelwood Cliffs, NJ, 1991.

[70] Sastry. S. S., *Nonlinear Systems: Analysis, Stability, and Control*, Springer, 1999.

APPENDICES

The expressions of $C_i (i = 1,\ldots,6)$ of eq. 3 are given in [13] as;

$$C_1 \equiv \sum_m \frac{\left[m^2 + \upsilon\left(\frac{a}{b}\right)^2\right]}{1-\upsilon^2} a^2 m$$

$$C_2 \equiv \sum_m \frac{\left[\left(\frac{a}{b}\right)^2 + \upsilon m^2\right]}{1-\upsilon^2} a^2 m$$

$$C_3 \equiv \sum_m \sum_s \sum_r a_m a_s a_r r^2 \{\alpha(s,m)\left[\gamma(s+m, r-n) - \gamma(s+m, r+n)\right] + \beta(s,m)\left[\gamma(s-m, r-n) - \gamma(s-m, r+n)\right]\}$$

where

$$\alpha(s,m) = \frac{m(s-m)}{\left[(s+m) + 4\left(\frac{a}{b}\right)^2\right]^2}$$

$$\beta(s,m) = \frac{m(s+m)}{\left[(s-m) + 4\left(\frac{a}{b}\right)^2\right]^2}$$

$$\gamma(s,m) = \text{ if } s = m = 0$$
$$= \text{if } s = m \neq 0$$
$$= \text{if } s \neq m$$

$$C_4 \equiv \sum_m \sum_s \sum_r a_m a_s a_r r^2 \{(s+m)\alpha(s,m)\left[\zeta(s+m, r+n) + \zeta(s+m, n-r)\right] + (s-m)\beta(s,m)\left[\zeta(s-m, r+n) + \zeta(s-m, n-r)\right]\}$$

where

$$\gamma(s,n) = \text{ if } s = n = 0$$
$$= \text{if } s = n \neq 0$$
$$= \text{if } s \neq n$$

$$C_5 \equiv \sum_m \sum_s \sum_r a_m a_s a_r r^2 \{(s+m)^2 \alpha(s,m)\left[\gamma(s+m,r-n)-\gamma(s+m,r+n)\right] + (s-m)^2 \beta(s,m)\left[\gamma(s-m,r-n)-\gamma(s-m,r+n)\right]\}$$

$$C_6 \equiv \sum_m \sum_s \sum_r a_m a_s a_r r^2 \{\frac{m}{s+m}\left[\gamma(s+m,r-n)-\gamma(s+m,r+n)\right] + \eta(s,m)\left[\gamma(s-m,r-n)-\gamma(s-m,r+n)\right]\}$$

where

$$\eta(s,m) = \frac{m}{s-m} \quad \text{if } s \neq m$$
$$= 0 \qquad \text{if } s = m$$